



This is a repository copy of *A 14000 year multi-proxy alluvial record of ecotone changes in a Fynbos-Succulent Karoo transition in South Africa.*

White Rose Research Online URL for this paper:

<https://eprints.whiterose.ac.uk/209685/>

Version: Accepted Version

---

**Article:**

Scott, L., Manzano, S., Carr, A.S. et al. (4 more authors) (2021) A 14000 year multi-proxy alluvial record of ecotone changes in a Fynbos-Succulent Karoo transition in South Africa. *Palaeogeography, Palaeoclimatology, Palaeoecology*, 569. 110331. ISSN 0031-0182

<https://doi.org/10.1016/j.palaeo.2021.110331>

---

Article available under the terms of the CC-BY-NC-ND licence  
(<https://creativecommons.org/licenses/by-nc-nd/4.0/>).

**Reuse**

This article is distributed under the terms of the Creative Commons Attribution-NonCommercial-NoDerivs (CC BY-NC-ND) licence. This licence only allows you to download this work and share it with others as long as you credit the authors, but you can't change the article in any way or use it commercially. More information and the full terms of the licence here: <https://creativecommons.org/licenses/>

**Takedown**

If you consider content in White Rose Research Online to be in breach of UK law, please notify us by emailing [eprints@whiterose.ac.uk](mailto:eprints@whiterose.ac.uk) including the URL of the record and the reason for the withdrawal request.



[eprints@whiterose.ac.uk](mailto:eprints@whiterose.ac.uk)  
<https://eprints.whiterose.ac.uk/>

1 **A 14 000 year multi-proxy alluvial record of ecotone changes in a Fynbos-Succulent Karoo**  
2 **transition in South Africa**

3 L. Scott<sup>1,\*</sup>, S. Manzano<sup>2</sup>, A. S. Carr<sup>3</sup>, C. Cordova<sup>4, 5</sup>, J. Ochando<sup>6</sup>, M. D. Bateman<sup>7</sup>, and J. S.  
4 Carrión<sup>6</sup>

5 1 Department of Plant Sciences, University of the Free State, Bloemfontein, South Africa

6 2 Plant Conservation Unit, Dept. Biological Sciences, HW Pearson Building, University of Cape  
7 Town, Private Bag X3, Rondebosch 7701, South Africa

8 3 School of Geography, Geology and the Environment, University of Leicester, University  
9 Road, Leicester, LE1, 7RH, UK

10 4 Department of Geography, Oklahoma State University, Stillwater, OK 74078, USA

11 5 Laboratory of Archaeology, Kazan Federal University, Kazan, Tatarstan, Russia

12 6 Department of Plant Biology, University of Murcia, Spain

13 7 Department of Geography, University of Sheffield, Winter St., Sheffield S10 2TN, UK

14

15 **Corresponding author**

16 *E-mail address:* [scottl@ufs.ac.za](mailto:scottl@ufs.ac.za) (L. Scott)

17 **Co-authors**

18 *E-mail addresses:* [saul.manzano.rodriguez@gmail.com](mailto:saul.manzano.rodriguez@gmail.com) (S. Manzano), [asc18@leicester.ac.uk](mailto:asc18@leicester.ac.uk)

19 (A. S. Carr), [carlos.cordova@okstate.edu](mailto:carlos.cordova@okstate.edu) (C. Cordova), [juan.ochando@um.es](mailto:juan.ochando@um.es) (J. Ochando),

20 [m.d.bateman@sheffield.ac.uk](mailto:m.d.bateman@sheffield.ac.uk) (M. D. Bateman), [carrion@um.es](mailto:carrion@um.es) (J. S. Carrión)

21

22 **Abstract**

23 To address long-standing questions concerning Southern Hemisphere climate dynamics and  
24 palaeoecological change in southern Africa, a Late Glacial-Holocene alluvial sediment  
25 sequence from the relatively dry interior year-round rainfall zone in South Africa was  
26 investigated. The study site borders the Fynbos biome and Succulent Karoo biome ecotone,  
27 and comprises a rare stratified sequence of sandy and organic-rich silt deposits, shown to  
28 span the last 14,000 years. A high resolution multi-proxy record of ecological change was  
29 derived using pollen, phytoliths and organic geochemical analyses. For the period 14-11 ka,  
30 significant valley aggradation occurred under relatively drier conditions, followed, during the  
31 early and middle Holocene, by alternating phases of humid and dry events with higher stream  
32 energy, slower accumulation or subtle seasonality changes. A transition from relatively humid  
33 to more arid conditions at 4-3 ka is identified and is consistent in timing with several interior  
34 year-round rainfall zone records. Results revealed alternations of fynbos and karroid elements  
35 and C<sub>3</sub>/C<sub>4</sub> grasses throughout the last fourteen thousand years, but did not suggest large-  
36 scale biome shifts. The record joins a growing number of sites contributing to debate over the  
37 complex atmospheric-oceanic drivers of palaeoclimate in this region. These data broadly fit  
38 to the regional pattern for the southernmost interior of South Africa in showing alternating  
39 influences from the westerly winter rain systems in the early Holocene, with a greater  
40 contribution from subtropical summer rain system during the middle and later Holocene.

41

42 **Key words:** Pollen, Southern Hemisphere, Younger Dryas, OSL, radiocarbon, seasonality

43

#### 44 **1. Introduction**

45 South Africa occupies an area under the influence of both the southern westerly  
46 winter rainfall and the subtropical (NE) summer rainfall systems of southern Africa (Taljaard,

47 1966; Tyson & Preston-Whyte, 2000) (Fig. 1). The dynamic transitional zone between these  
48 rainfall regimes lies broadly across the boundary between the Eastern and Western Cape  
49 Provinces (Figure 1), generating an essentially year-round rainfall regime, which combined  
50 with marked patterns in geological substrate and topography, also produces sharp ecotones  
51 between major southern African biomes; namely the Fynbos, Succulent Karoo, Nama Karoo  
52 and Albany Thicket Biomes (Mucina and Rutherford, 2006).

53

54 It is long-recognised that an understanding of the dynamics of the summer-winter-  
55 transitional rainfall zones of southern Africa will inform our wider understanding of Southern  
56 Hemisphere climate and biodiversity dynamics (van Zinderen Bakker, 1967; Chase and  
57 Meadows, 2007, Chevalier and Chase, 2015). Despite the known challenges of  
58 palaeoecological research in these arid -to semi-arid environments, there is a steadily growing  
59 number of palaeoecological sites from the Cape inland and coastal regions. Notable examples  
60 are the pollen records from the Nama Karoo Biome to the north at Blydefontein (Scott et al.,  
61 2005, 2012, 2020, in prep.) and isotope, charcoal, pollen, microfauna records from the Albany  
62 Thicket and Fynbos Biomes to the south-east and west; viz Baviaanskloof (Chase et al., 2020),  
63 the Cango Valley (Cango Caves and Caves and Boomplaas (Scholtz, 1986; Talma and Vogel,  
64 1992; Thackeray, 1987; Faith et al., 2018) and Seweweekspoort (Chase et al., 2017) (Fig. 1 A).  
65 There are also studies on the history of the coastal area in the Fynbos Biome at Norga (Scholtz,  
66 1986); Vankervelsvlei (Quick et al., 2016), Groenvlei (Martin, 1968), Eilandvlei (Quick et al.,  
67 2018); Still Bay (Rietvlei) (Quick et al., 2015) and further to the west at Princessvlei (Neumann  
68 et al., 2011; Cordova et al., 2019). Along the west coast to the north, there are pollen and  
69 isotope records from the fynbos biome in the Cederberg (Scott and Vogel, 2000; Scott and  
70 Woodborne, 2007a, b; Quick et al., 2011, Valsecchi et al., 2013, Chase et al., 2015) and from

71 more distant sites like Pella and Eksteenfontein in the Succulent Karoo and Desert Biomes,  
72 respectively (Scott, 1996; Lim et al., 2016) (Fig. 1A).

73

74 Further integrative works i.e., Chase and Meadows (2007), Chase et al. (2013); Chase  
75 et al. (2020) and Chase and Quick (2018), have sought to summarize the Quaternary variability  
76 in both ocean and atmospheric circulation systems and their impact on southern African  
77 climate. Long-term macro-scale climatic influences include a variety of forcing mechanisms  
78 e.g., precession or extent of Atlantic sea ice (Berger and Loutre, 1991; Street-Perrott and  
79 Perott, 1993; Nielson et al., 2004; Fischer et al., 2007; Chase et al., 2013). Recently, Chase  
80 and Quick (2018) argued that in contrast to the adjacent interior, the primary driver of climatic  
81 change in the southern coastal zone, was the localised coastal influence of the Agulhas  
82 Current. Subsequently, Chase et al. (2020) presented further evidence for a coastal-  
83 continental interior dichotomy in Holocene climatic trends and time scales. These studies  
84 emphasise the need for a detailed network of palaeo-archives to properly untangle regional  
85 palaeoclimatic dynamics in this physiographically complex and yet critical climatic/ecological  
86 transition zone. The available records need to be better integrated with each other to  
87 interrogate such models of ocean and atmospheric circulation patterns.

88

89 We have identified several new sites of palaeoecological interest in valleys of the  
90 topographically complex eastern Little Karoo between the Great Karoo and southern Cape  
91 Fold Belt Mountains near Uniondale (Fig. 1). These comprise extensive (typically 3-10 m thick)  
92 alluvial valley-fills containing stratified sequences of organic-rich and sandy fluvial sediment  
93 set within and at the margins of the major mountain fronts. Some of these sequences were  
94 exposed by flash flooding in 2007, presenting hitherto under-examined archives of

95 environmental change and landscape response, which can potentially identify environmental  
96 changes if studied in sufficient detail over the wider region before they will eventually be lost  
97 by future erosion (e.g. Bousman et al., 1988; Cohen and Nanson, 2007). One of these exposed  
98 alluvial deposits in the Kamanassie River, henceforth referred to as the KMR sequence (Fig.  
99 1), is the subject of this study. We report the site chronology, as derived with radiocarbon and  
100 optically stimulated luminescence (OSL) dating, as well as a complete suite of geochemical,  
101 phytolith and palynological data. We view the results in relation to the current vegetation  
102 types and ecotones in the region and their pollen production in the Succulent Karoo and  
103 Fynbos Biomes (Figure 1) and compare the new results to the nearest key records to  
104 understand the local processes in the formation of the KMR site.

105

## 106 **2. Setting**

107 The KMR study site (Fig. 1) is surrounded by areas experiencing semi-arid to sub-humid  
108 climates with a suite of geological substrates, resulting in complex biome and vegetation  
109 patterns (Fig. 1). The area lies within the all year rainfall region (Taljaard, 1966; Tyson and  
110 Preston-Whyte, 2000) receiving ~615 mm rain annually, with slightly lower precipitation  
111 during winters than autumns and springs (Mucina and Rutherford, 2006) and with occasional  
112 frost in winter (~13 days per year). The mean annual temperature is 15.8 °C (Tyson and  
113 Preston-Whyte, 2000).

114

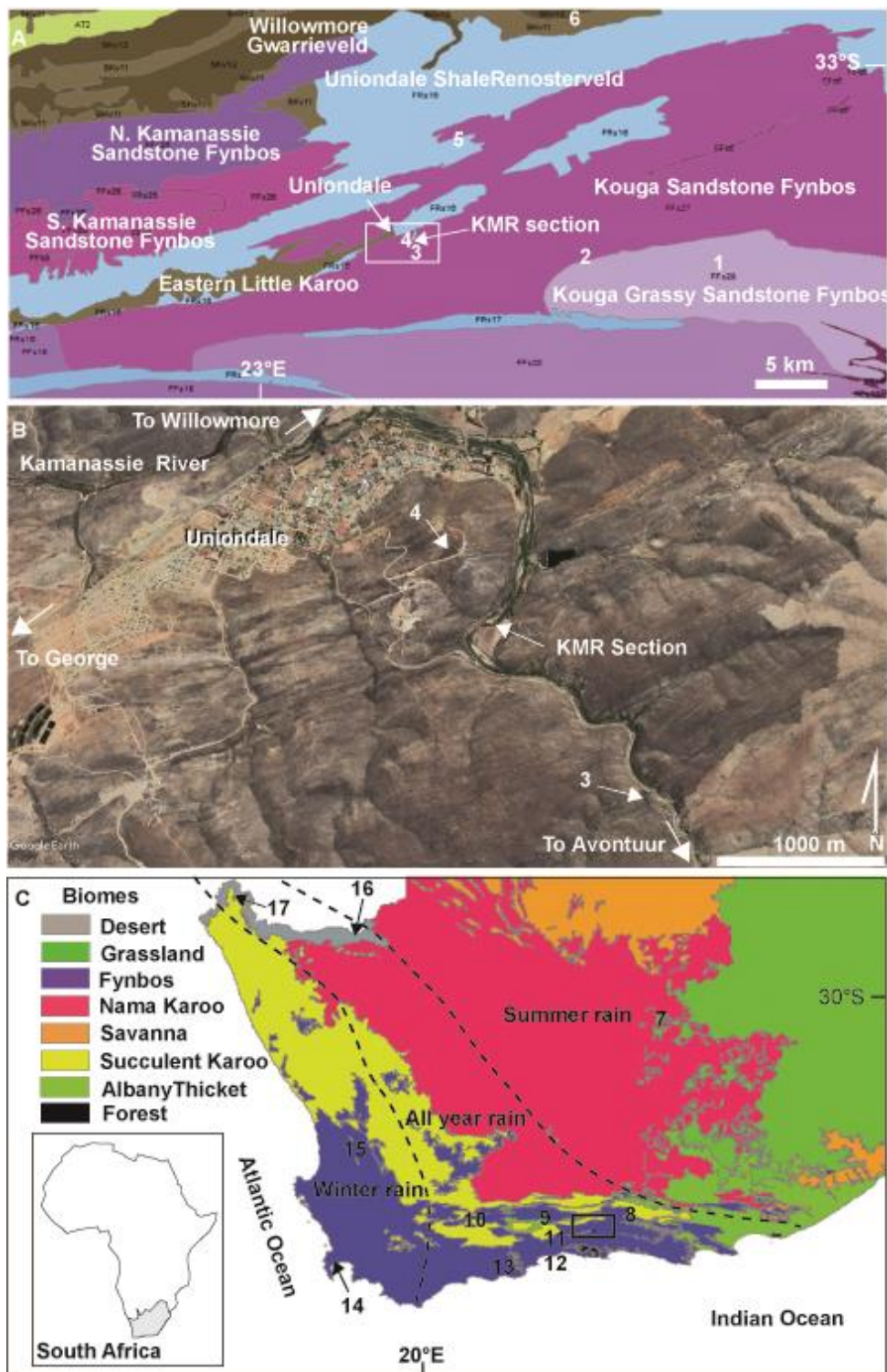
115 The studied alluvial deposits lie at ~870 m altitude, in the Fynbos Biome in the Eastern  
116 Fynbos Renosterveld Bioregion (F06) (Mucina and Rutherford, 2006) (Fig. 1) (-33.66561 S,  
117 23.1362 E). They have formed as a valley fill in the Kamanassie River. The catchment of this

118 drainage line starts in fynbos and runs towards more karroid vegetation before eventually  
119 turning west towards the Gourits River (Fig. 1 A, B. and C.). The site is bordered to the north  
120 by Uniondale Shale Renosterveld and to the south by the montane Kouga Sandstone Fynbos.  
121 To the west and north Patches of Eastern Little Karoo belonging to the Succulent Karoo Biome  
122 occur immediately west of the site and further to the north several kilometres away (Mucina  
123 and Rutherford, 2006).

124

125           In view of this setting special consideration in interpretations must be given to fluvial  
126 transport of organic matter and microscopic material, including pollen, phytoliths and organic  
127 debris, which are not necessarily of local origin. However, they are likely derived from within  
128 the relatively small Kamanassie River catchment within the Kouga Mountains south of  
129 Uniondale. Flood events, fluvial transport, standing water phases, fire and rainfall seasonality  
130 all potentially play a role in the deposition and preservation of the organic material relating  
131 to past environments of the area.

132



133

134 Fig. 1. A. Vegetation types (Mucina and Rutherford, 2006) with numbers 1 to 6 indicating the

135 locations of modern surface pollen samples (see Supplemental Material) location of the KMR

136 site (rectangle covers B). B. Locality of the studied KMR Section with the nearest modern

137 samples (3 and 4). C. Biome map (Mucina and Rutherford, 2006) with the study area



138 (rectangle covers A) and key palaeoenvironmental sites in the region: 7 Blydefontein, 8  
139 Baviaanskloof, 9 Cango Caves/Boomplaas, 10 Seweweekspoort, 11 Norga/Vankersvelsvlei, 12  
140 Groenvlei/Eilandvlei, 13 Rietvlei /Still Bay, 14 Princes Vlei, 15 Cederberg, 16 Pella, 17  
141 Eksteenfontein.

142

### 143 **3. Methods**

144 Samples were recovered directly from the exposed face of the deposit. The same  
145 sampled materials were utilised for geochemical, phytolith and pollen analyses, with  
146 exceptions depending on the productivity of different proxy types, or the need for specific  
147 focus on a particular proxy. The site stratigraphy was logged in detail and 61 samples obtained  
148 for analysis indicated in Fig. 2A and a photograph showing the general nature of the section  
149 appear in Fig. 2B.

150

#### 151 *3.1. Dating*

152 Two laboratories, viz., <sup>14</sup>Chrono at Queen's University, Belfast and the Accelerator  
153 Mass Spectrometry Laboratory at the University of Arizona, Tucson, provided eleven AMS  
154 dates for the sequence (two from the east section (Site 1) and nine from the main section  
155 (Site 2). They comprised one <sup>14</sup>C analysis on bulk organic matter sample, three on pollen  
156 extractions and seven on charcoal samples (Table 1). Additionally, optically stimulated  
157 luminescence (OSL) ages for three sandy layers using coarse grained quartz, were undertaken  
158 at the Sheffield University luminescence laboratory one from Site 1 and two from Site 2, (see  
159 Table 2 and Supplementary Material for more on the OSL dating methods).

160

#### 161 *3.2. Biogeochemistry*

162 Forty samples were analysed for their Total Nitrogen (TN), Total Organic Carbon (TOC)  
163 contents and their  $\delta^{13}\text{C}_{\text{TOC}}$  values to investigate the organic matter composition. To account  
164 for the presence of geogenic carbon (carbonate), samples were analysed with (TOC and  
165  $\delta^{13}\text{C}_{\text{TOC}}$ ) and without (TN) acid treatment. The acid-insoluble residue (TOC) is considered the  
166 best representation of the organic carbon present in the sediments and the carbon isotope  
167 composition ( $\delta^{13}\text{C}_{\text{TOC}}$ ) was obtained from this material (See Supplemental Material for  
168 methods).

169

### 170 3.3. *Microfossil extraction*

171 For investigation of the vegetation history, residues for pollen, non-pollen palynomorphs  
172 (NPPs) and phytolith analysis were prepared using standard extraction methods (Faegri and  
173 Iversen, 1989), including sodium polytungstate heavy liquid separation (specific gravity 2.3)  
174 (Munsterman and Kerstholt, 1996). The microscope slides were mounted in glycerine-jelly  
175 and duplicates used for phytolith identification and palynology.

176

### 177 3.4. *Phytoliths*

178 A minimum of 300 phytoliths were counted on each slide and phytolith concentration  
179 was calculated using *Lycopodium* marker spores (Stockmarr, 1971). Phytolith counts were  
180 divided into graminoid and non-graminoid, excluding those that could not be assigned to any  
181 group. The classification of phytoliths follows a modified version of previous research in the  
182 region (see Supplemental Material Figs. S2&3 for more on methods and classification). Using  
183 different phytolith groups and their taxonomic associations, several ratios provide a basis for  
184 characterizing vegetation communities along with pollen. The non-graminoid-to-graminoid  
185 ratio represents the proportions of plants that do not belong to grass-like plants and provides

186 an idea of closed shrub canopy versus open grassy spaces. Additionally, the Poaceae-  
187 Restionaceae ratio, suggests the presence of restioid fynbos.

188 The grass silica short cell phytolith (GSSC) ratios indicate the relative abundance of C<sub>3</sub>  
189 and C<sub>4</sub> grasses. The C<sub>3</sub>/C<sub>4</sub> ratio was obtained by dividing the sum of C<sub>3</sub>-diagnostic GSSC by the  
190 sum of all C<sub>4</sub>-diagnostic GSSC. As C<sub>3</sub> grasses are abundant in the winter-rainfall zone of South  
191 Africa (Vogel et al., 1978), a mirror ratio, the C<sub>4</sub>/C<sub>3</sub>×100 GSSC ratio, is used to more clearly  
192 visualise the representation of C<sub>4</sub> grass.

193

### 194 3.5. *Paleofire proxies*

195 Burned Poaceae phytoliths, presented here as percent of the total Poaceae phytoliths,  
196 provide a proxy for grass fires (as opposed to overall fires as indicated by microscopic  
197 charcoal; Cordova et al. 2019). Two different methods of microscopic charcoal estimation  
198 were used during the phytolith and palynological analyses, with the former presented here  
199 as viz., counts per mm<sup>2</sup> and the latter as counts per gram following the addition of spikes the  
200 same *Lycopodium* spores (Stockmarr, 1971) used for concentration estimates in the  
201 palynological study (see *Palynology* below and in the Supplemental Material).

202

### 203 3.6 *Palynology*

204 A minimum of 300 pollen grains from terrestrial plants, plus, aquatics, spores and non-  
205 pollen palynomorphs (NPPs including fungal spores and algae) was identified from forty-four  
206 productive layers (usually the grey-brown sands with organic material). The light-coloured  
207 coarse-grained sands and gravels preserved insufficient pollen. Pollen zones I-V were  
208 obtained by CONISS (Grimm, 2011) based on the terrestrial taxa.

209

210 Modern surface samples were analysed to assess the modern pollen production for both  
211 fynbos and karroid vegetation types (Mucina and Rutherford, 2006) (Fig. 1). Six modern  
212 surface-soil samples from near the site and in two transects of ~30 km in different directions  
213 away to the south-east along the Kouga Mountains and north-east towards Willowmore,  
214 were collected (Fig. 1B) (see Supplemental Material for details and results).

215

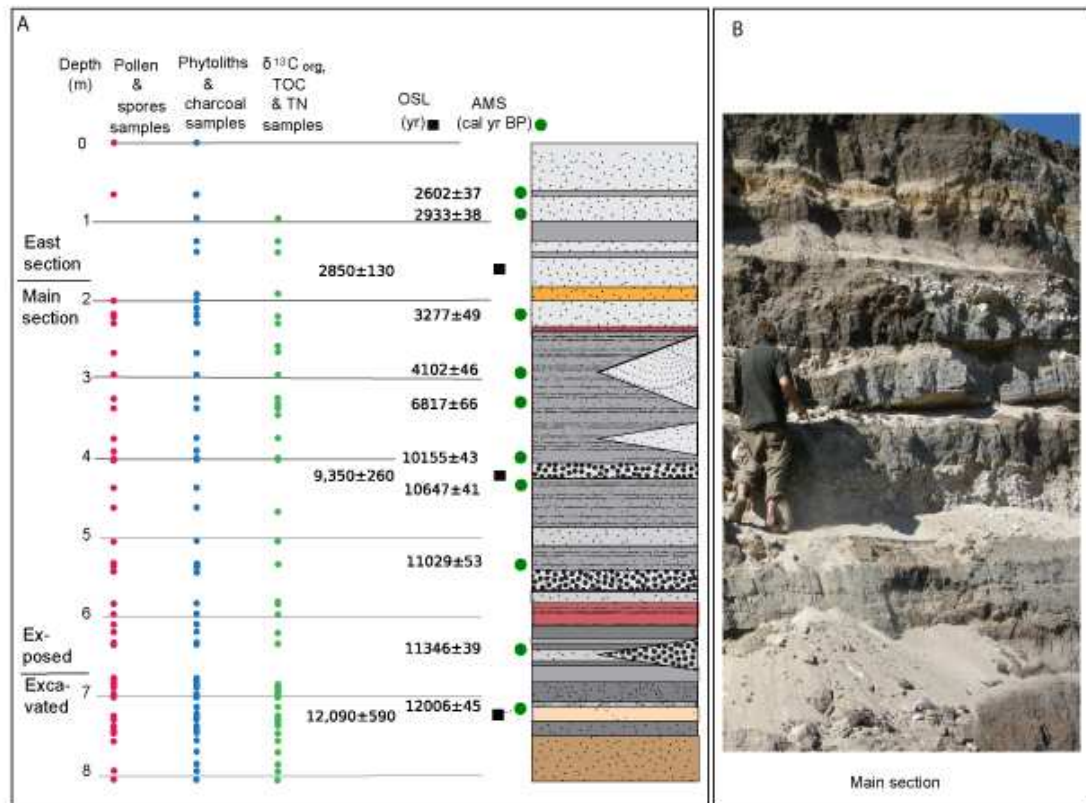
## 216 **4. Results**

### 217 *4.1. Description of the sequence of deposits*

218 The sequence comprises of a series of distinct, alternating sedimentary units of  
219 organic, fine-grained wetland, to coarse-grained sandy and mineral-rich gravelly layers (Fig.  
220 2A, Table 1).

221

222



223

224 Fig. 2. A. Combined lithological profile of the eastern and main sections. Dots on the left  
 225 indicate sample positions, of which not all levels were necessarily productive. B. View of the  
 226 main section with M. Wessels standing at the c. 5.8 meter level.

227

228 Table 1. KMR profile description

<b>KMR sections</b>	<b>Depth (cm)</b>	<b>Description</b>
<b>East</b>	0-180	Organic rich silts/fine sands with rootlets, prominent more organic layers at c. 65, 95, 126 and 135 cm (OSL 2.8 ka, 165 cm)
<b>Main</b>	180-200	Iron stained, coarse sands that pinch out laterally
	200-230	Dark silts below prominent iron stained layer
	235	Prominent reddish sands
	240-405	Laminated grey/black silty sands, rich in organic matter with lenses of coarse sands/gravel and some pebbles that pinch in and out with some vestiges of bedding that can be traced laterally but tend to pinch out
	405-423	Pebble layer (top is the datum) (OSL 9.4 ka, 4.2 cm)
	425-486	Laminated grey/black silty sands, rich in organic matter
	486-510	Clean (inorganic), coarse sand/some gravel
	510-540	Laminated grey/black silty sands, rich in organic matter, gravel and coarse sand
	540-568	Coarse, quartz-rich laminated sands
	568-583	Grey/brown laminated organic-rich silts, some reddish staining
	583-610	Prominent black silts rich in organic matter
	610-624	Grey/brown laminated organic-rich silts, some reddish staining
	624-665	Grey/brown laminated organic rich silts, some reddish staining above black organic rich clays and coarse sands with a gravel lens that pinches out laterally

	665-685	Coarse grey/brown sand grading downwards over 2-3 cm to grey/black sands
	685-705	Grey/black coarse sands
	710	Dark brown silty fine sands
	712-730	Orange mottled, fine sands (OSL 12.1 ka, 722 cm)
	730-752	Black, water-saturated sands
	752-806	Brown mottled coarse sands

229

230 *4.2. Dating*

231 The radiocarbon dating results are presented in Table 2 and OSL sample list and results  
 232 in Tables 3 and 4 respectively. The resulting age model obtained using Bacon and the SHcal13  
 233 curve (Blaauw and Christen, 2011; Hogg et al., 2013) is shown in Figure 3. Because the  
 234 calibrated radiocarbon ages are expressed as cal yr BP and the OSL as years, ages in  
 235 subsequent plots of proxy data are expressed as modelled age (yr).

236

237 Table 2. Radiocarbon dates from the KMR Section.

Sample ID	Material	Age (yr BP)	Error (yr)	Depth (cm)	Cal yr BP (2 sigma ranges)	$\delta^{13}\text{C}_{\text{org}}$ (‰)
UBA-20534	Pollen	2583	37	65	2471-2602-2747	-26.3
UBA-20533	Pollen	2960	38	95	2925-2933-3168	-21.6

AA90910	Charcoal	3123	49	220	3141-3277-3391	-26.7
AA90909	Charcoal	3800	46	295	3963-4102-4247	-26.5
UBA- 20532	Pollen	6030	66	325	6659-6817-6984	-27.3
UBA- 18270	Charcoal	9060	43	400	10121-10155-10246	-28.5
UBA- 20337	Charcoal	9473	41	430	10541-10647-10754	-25.7
AA90133	Organics	9736	53	463	11063-11029-11223	-26.3
UBA- 20338	Charcoal	9865	43	537	11170-11225-11311	-29.0
UBA- 18269	Charcoal	9977	39	640	11228-11346-11411	-25.7
UBA- 18271	Charcoal	10311	46	715	11763-12006-12155	-19.8

238

239 Table 3. OSL sample list for KMR section.

Field code	Sample code	Depth from surface (m)
KMR10/1/3 Site 1	Shfd10083	1.65
KMR10/1/1 Site 2	Shfd10081	4.20
KMR10/1/2 Site 2	Shfd10082	7.22

240

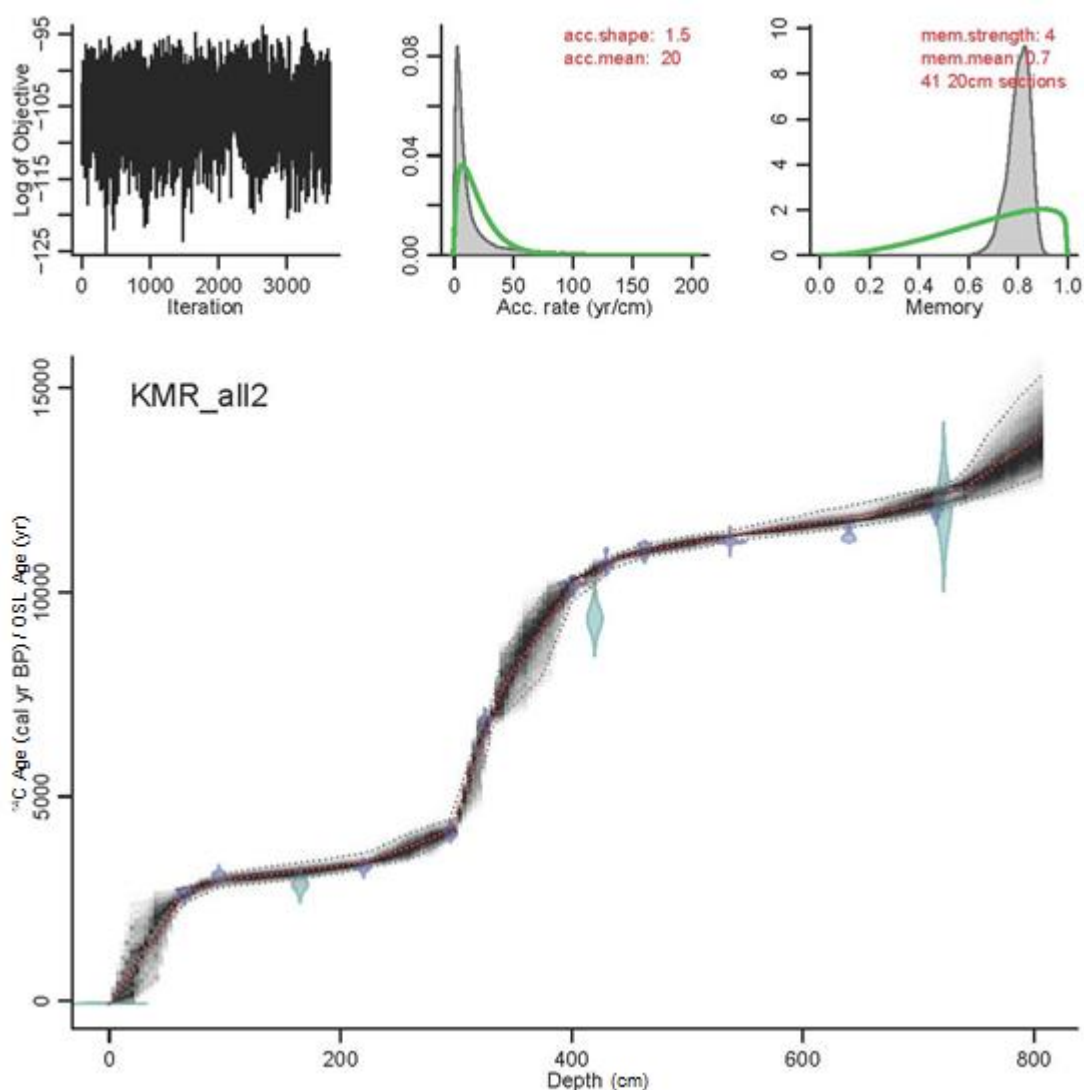
241



242 Table 4. OSL related data for KMR section.

Depth (m)	Water content (%)	K (%)	U (ppm)	Th (ppm)	Cosmic dose rate (Gy kyr <sup>-1</sup> )	Total dose		Age (C.E.)
						rate (Gy kyr <sup>-1</sup> )	D <sub>e</sub> (Gy)	
1.65	0.1	0.1	0.98	1.93	0.18 ± 0.01	0.71 ± 0.03	2.04 ± 0.05	2890 ± 140
4.20	0.2	0.3	1.00	4.06	0.13 ± 0.01	1.00 ± 0.04	9.36 ± 0.26	9360 ± 440
7.22	11.1	0.1	0.57	3.69	0.12 ± 0.01	0.60 ± 0.02	7.26 ± 0.25	12030 ± 590

243



244

245 Fig. 3. Bacon age model using Blaauw and Christen (2011). Radiocarbon dates: light blue; OSL

246 dates: light blue-green.

247

248           The radiocarbon chronology of the eight-meter KMR sequence is reasonably well  
249 supported by the three OSL ages, showing that deposition started around 14000 years ago  
250 before the Younger Dryas (YD) event. The age-depth model suggests varying sedimentation  
251 rates with faster accumulation, implying phases of marked valley fill aggradation from 14000  
252 to 11000 years ago and between 4000 and 3000 years ago, with slower accumulation  
253 between 7000 and 4000 years ago and during the last 2500 years. The latter phases also have  
254 low proxy sample resolution due to their low organic contents.

255

#### 256 *4.3 Geochemistry*

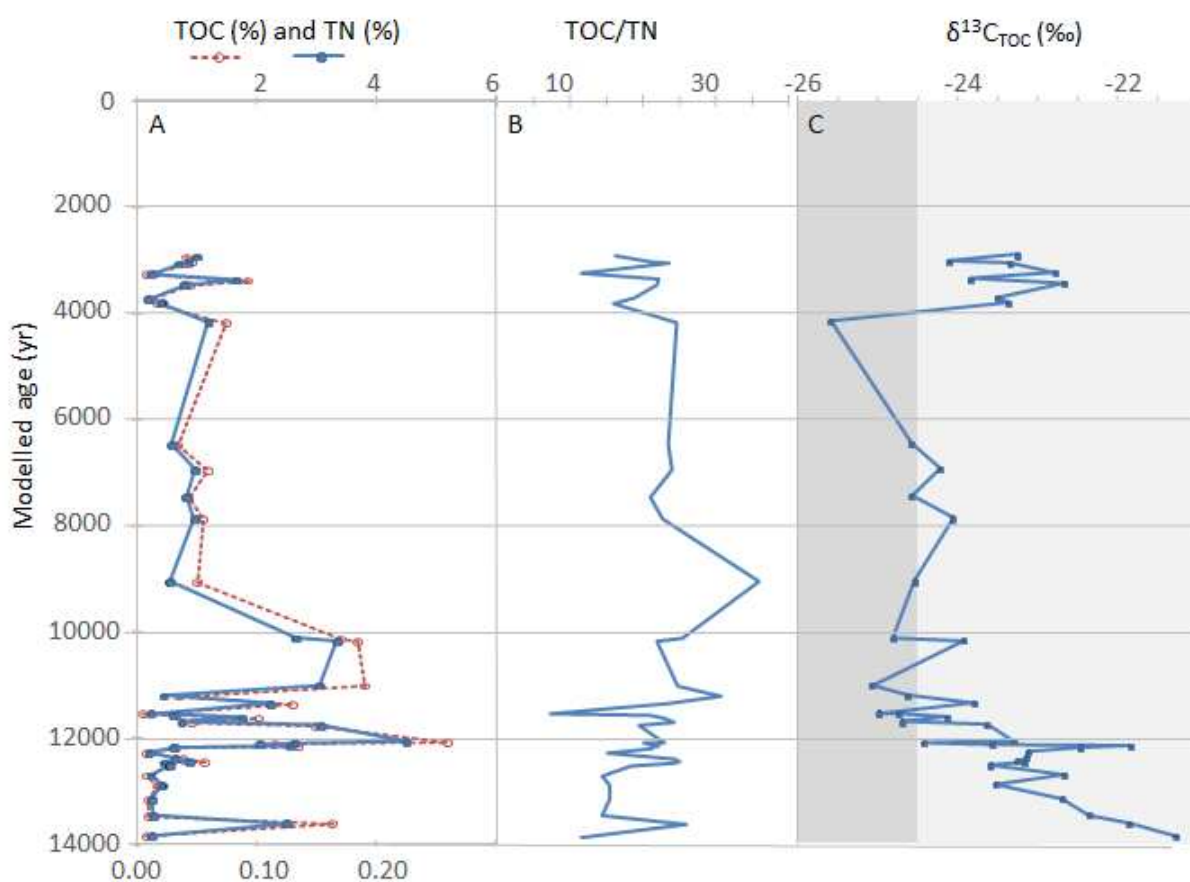
257           The total organic carbon content is highly variable, ranging from 0.1 to 5.2% (Fig. 4A).  
258 Although obviously inorganic sand layers were not sampled for organic geochemical analysis,  
259 the down-section variation in TOC does largely track the sedimentary facies within the  
260 section, with the highest TOC values generally associated with dark coloured silts and silty  
261 sands (e.g. 4.68, 5.35, 6.87 m, associated ages of 11 ka, 11.3 ka and 12 ka ). TN closely tracks  
262 TOC (Pearson's  $R = 0.99$ ), suggesting the former is most likely organic N. The TOC/TN ratio  
263 ranges between 36 and 7 (Fig. 4B), but largely falls in the range 10-25 (mean =  $21 \pm 5$ ). The  
264 two outlier TOC/TN values at 9.0 and 11.5 ka are associated with TN contents  $< 0.03\%$  and are  
265 potentially impacted by measurement imprecision at such low N contents. Except for these  
266 two outlier values, there are no trends in TOC/TN through the sequence; the Late Holocene  
267 (2.9-3.8 ka) mean TOC/TN ( $21 \pm 4$ ) is identical to that of the Late Glacial (11.5-13.8 ka;  $20 \pm 4$ ).  
268 In the more sporadically preserved early to mid-Holocene section (11.3-6.5 ka) the average  
269 ratio is marginally higher ( $25 \pm 5$ ), but the significance of this is hard to evaluate given the  
270 limited number of samples.

271

272 The  $\delta^{13}\text{C}_{\text{TOC}}$  ranges between -25.6 and -21.3 ‰ (Fig. 4C) with some clear trends  
273 apparent. From a sequence maximum of -21.3 ‰ at the base of the sequence (13.8 ka)  $\delta^{13}\text{C}_{\text{TOC}}$   
274 declines steadily (with a brief rise to -21.8 ‰ at 12.1 ka) to -25 ‰ at 11.0 ka, whereupon it  
275 remains relatively stable to 6.5 ka (-24.4 ± 0.4 ‰). In the late Holocene section (3.8-3.0 ka)  
276  $\delta^{13}\text{C}_{\text{TOC}}$  is higher than the early to mid-Holocene and is clustered at -23.7 ± 0.9 ‰. The precise  
277 timing of this late Holocene shift to higher  $\delta^{13}\text{C}_{\text{TOC}}$  is difficult to determine given the limited  
278 number of mid to late Holocene samples, although the  $\delta^{13}\text{C}_{\text{TOC}}$  of the immediately subjacent  
279 sample at ~4.2 ka is lower (-25.6 ‰) than those above it.

280

281



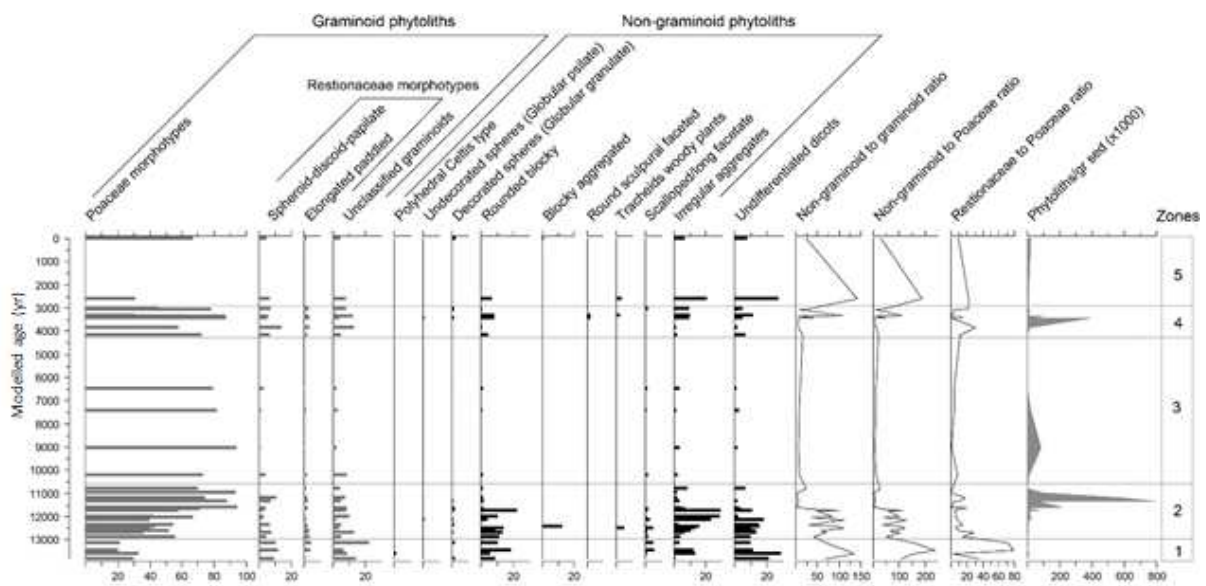
282

283 Fig. 4. A. TOC (red/dashed, top scale) and TN (blue, bottom scale). B. TOC/TN. C. Down-section  
 284 trends in  $\delta^{13}\text{C}_{\text{TOC}}$ . Dark and light shades indicate measured ranges of typical soil  $\delta^{13}\text{C}_{\text{TOC}}$  from  
 285 the Fynbos and Succulent Karoo Biomes respectively (Carr et al., in prep).

286

287 **4.4 Phytoliths**

288 The distribution of silica phytolith morphotypes varies considerably, but they are best  
 289 preserved in zones 1, 2 and 4 (Fig. 5 and 6). These changes are divided into five zones.



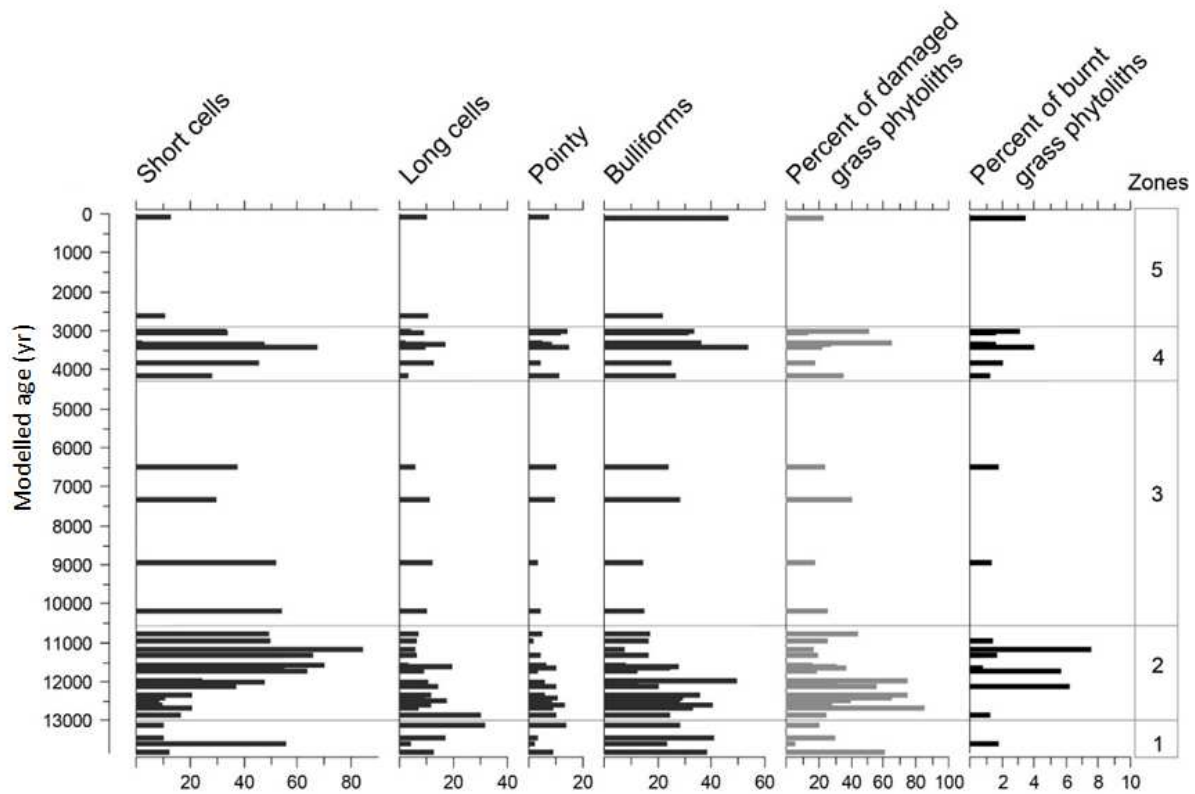
290

291 Fig. 5 Phytolith groups, summary and ratios.

292

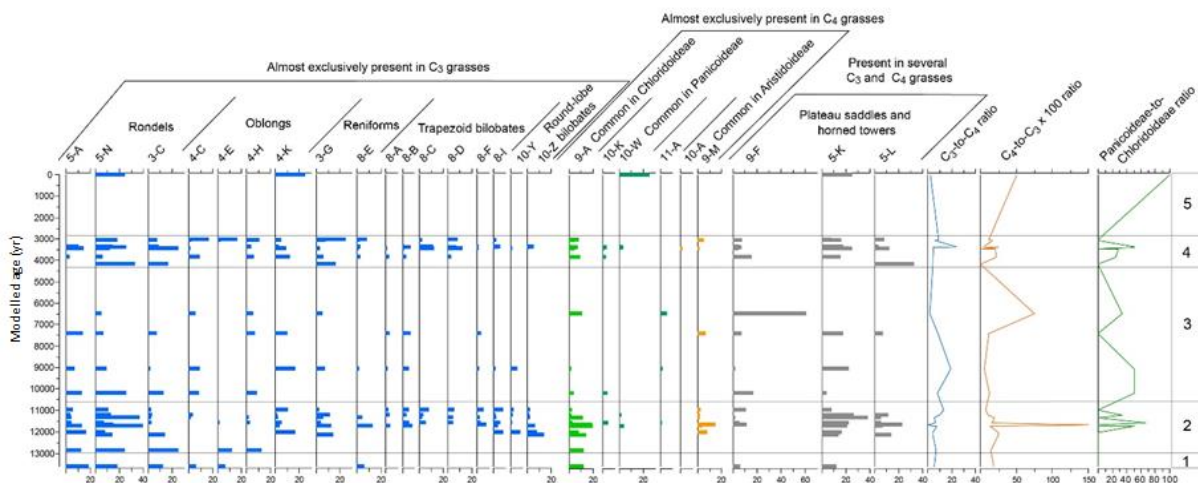
293 Although with relatively low counts, Phytolith zone 1 (14-12.9 ka) shows a clear  
 294 dominance of non-graminoids over graminoids (Figure 5). For the latter, the incidence of  
 295 Poaceae is lower than Restionaceae and unclassified graminoids. Poaceae phytoliths are  
 296 highly variable through the zone, and the percent of burnt phytoliths is low (Fig. 6). GSSC show  
 297 approximately equal abundances of C<sub>3</sub> and C<sub>4</sub> grasses, with the latter always exclusively the  
 298 Chloridoideae (Fig. 7).

299



300

301 Fig. 6. Poaceae phytoliths and percent of burnt grass phytoliths.



302

303 Fig. 7. Grass silica short cells (GSSC) and ratios.

304

305 Phytolith zone 2 (12.9-10.6 ka) shows a gradual increase of graminoids over non-  
 306 graminoids (Fig. 6 and 7). Within the graminoids, Poaceae increase relative to Restionaceae  
 307 phytoliths (Fig. 5). Within Poaceae short cells become increasingly more abundant towards

308 11 ka, suggesting perhaps better preservation or higher phytolith input by wind (Fig. 6). Burnt  
309 grass phytoliths also increase towards 11 ka, reaching their highest abundance for the  
310 sequence, and they suggest an increase of grass fires. In the GSSC, the proportion of C<sub>3</sub> vs. C<sub>4</sub>  
311 remains the same as phytolith zone 1, except for a single-sample peak in C<sub>4</sub> and a relative  
312 increase in Panicoideae diagnostic GSSC at c. 12 ka (Fig. 7).

313

314 Phytolith zone 3 (8.2-3 ka) is associated with few samples that preserve plant silica,  
315 probably reflecting the coarser sediment texture. However, it shows a general distribution of  
316 phytolith groups like the top of zone 2, with graminoids dominating over non-graminoids, and  
317 Poaceae dominant over Restionaceae. Similarly, the proportions of Poaceae morphotypes  
318 remain relatively unchanged, with short cells dominating alongside a marked reduction in the  
319 percentage of burnt grass phytoliths (Fig. 6). The GSSC also show notable changes across the  
320 zone (Fig. 7). Before 6 ka C<sub>3</sub>-diagnostic GSSC dominate, while among the C<sub>4</sub> the Panicoideae  
321 remain significant. After 6 ka, the proportions of C<sub>3</sub> decline in favour of C<sub>4</sub>, and among the  
322 latter Chloridoideae becomes dominant over Panicoideae.

323

324 Phytolith zone 4 (3-1.9 ka) shows a moderate incidence of non-graminoids over  
325 graminoids, and of Restionaceae over Poaceae (Fig. 5). Among Poaceae phytoliths,  
326 dominance fluctuates between short cells and bulliforms, while the percent of burnt grass  
327 phytoliths increases. The proportions of C<sub>3</sub> and C<sub>4</sub>-diagnostic GSSC indicates an increase in C<sub>3</sub>,  
328 while within the C<sub>4</sub>-diagnostic GSSC the proportions of Panicoideae dominate over  
329 Chloridoideae at times.

330

331 Phytolith zone 5 (from 1.9 ka onwards) consists of two samples. Notably the  
332 proportions of graminoids and Poaceae are higher in the top sample, (Fig. 5), with bulliforms  
333 dominating among the Poaceae (Fig. 6). The top sample shows a codominance between C<sub>3</sub>  
334 and C<sub>4</sub>, with the latter dominated entirely by Panicoideae.

335

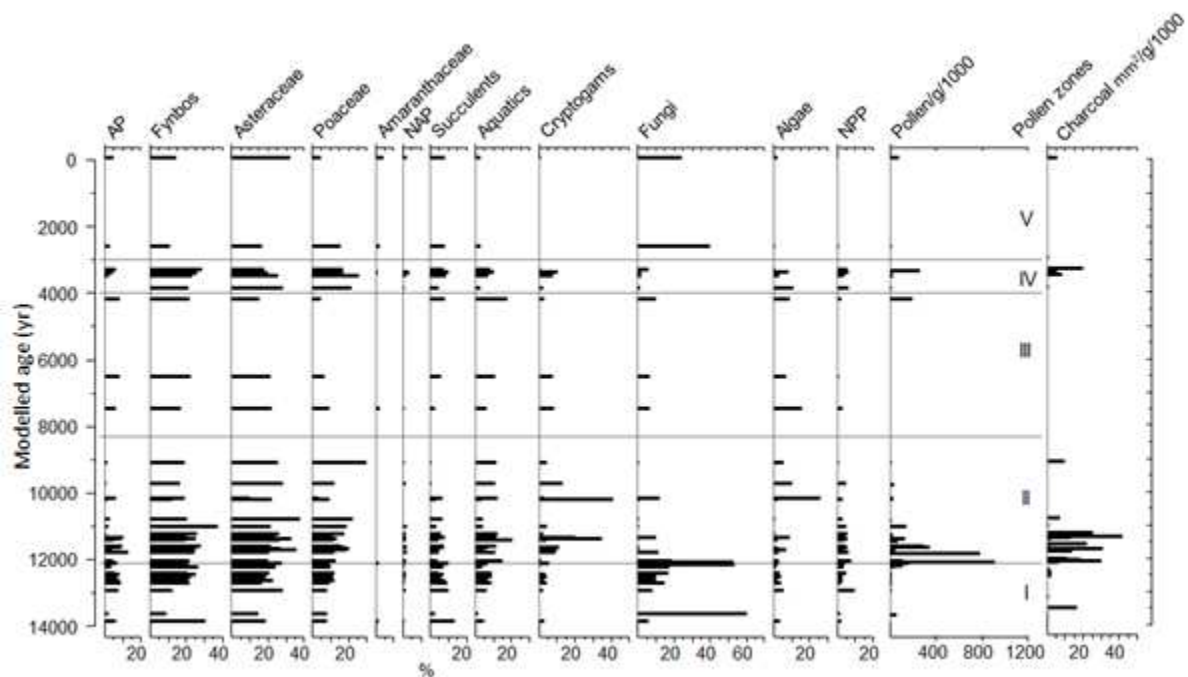
#### 336 4.5. Paleofire proxies

337 The results of the two methods of micro-charcoal determination record the same  
338 trend, with an apparent peak in fire at ~11.5 ka, lower intensity of fire until the late Holocene,  
339 followed by a second peak at c. 4 ka (Fig. 8 and Fig S4 for size classes).

340

#### 341 4.6. Palynology

342 Pollen concentrations in KMR section were highly variable and highest pollen  
343 concentrations occurred in the samples at c. 12 ka (Fig. 8).



344

345 Fig. 8. Summary diagram of percentages of all palynomorph types. AP = arboreal pollen,  
346 NAP=other non-arboreal pollen, NPP = non-pollen palynomorphs. The columns on the right  
347 show pollen and microscopic charcoal concentrations (size classes in Fig. S4) and pollen zones  
348 (for creation of zones, see Fig. 9).

349

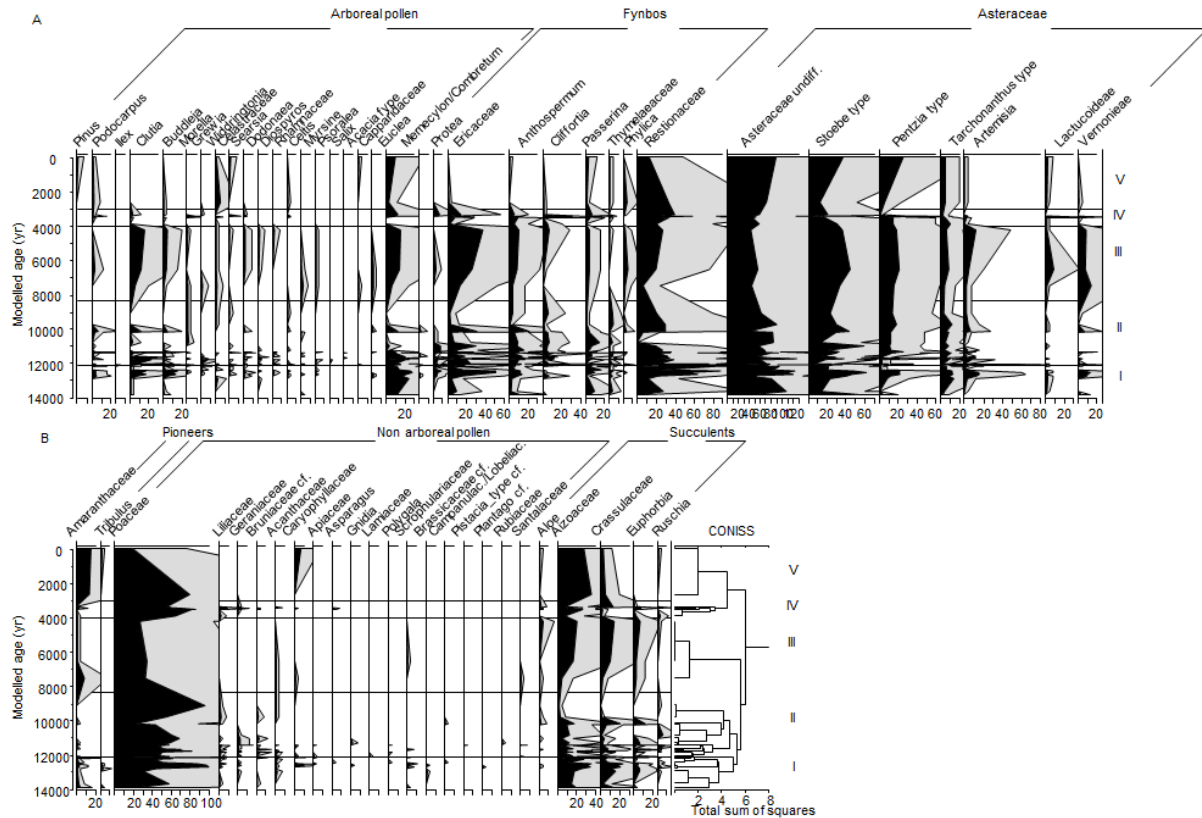
350 Pollen characteristic of fynbos vegetation, as well as Asteraceae, Poaceae and  
351 succulent pollen groups are prominent throughout the sequence. Variability across numerous  
352 individual pollen types is high at some levels in the sequence. Despite distinctive changes in  
353 the individual pollen types, the relative abundance of these groups is largely consistent,  
354 suggesting relatively subtle changes in vegetation over the studied interval (Fig. 9 and 10).  
355 Apart from the regional pollen (Fig. 9), we observe variations in other palynomorphs (Fig. 10)  
356 of aquatic pollen types, cryptogam spores, fungal spores and algae (local palynomorphs and  
357 NPPs).

358

359

360





361

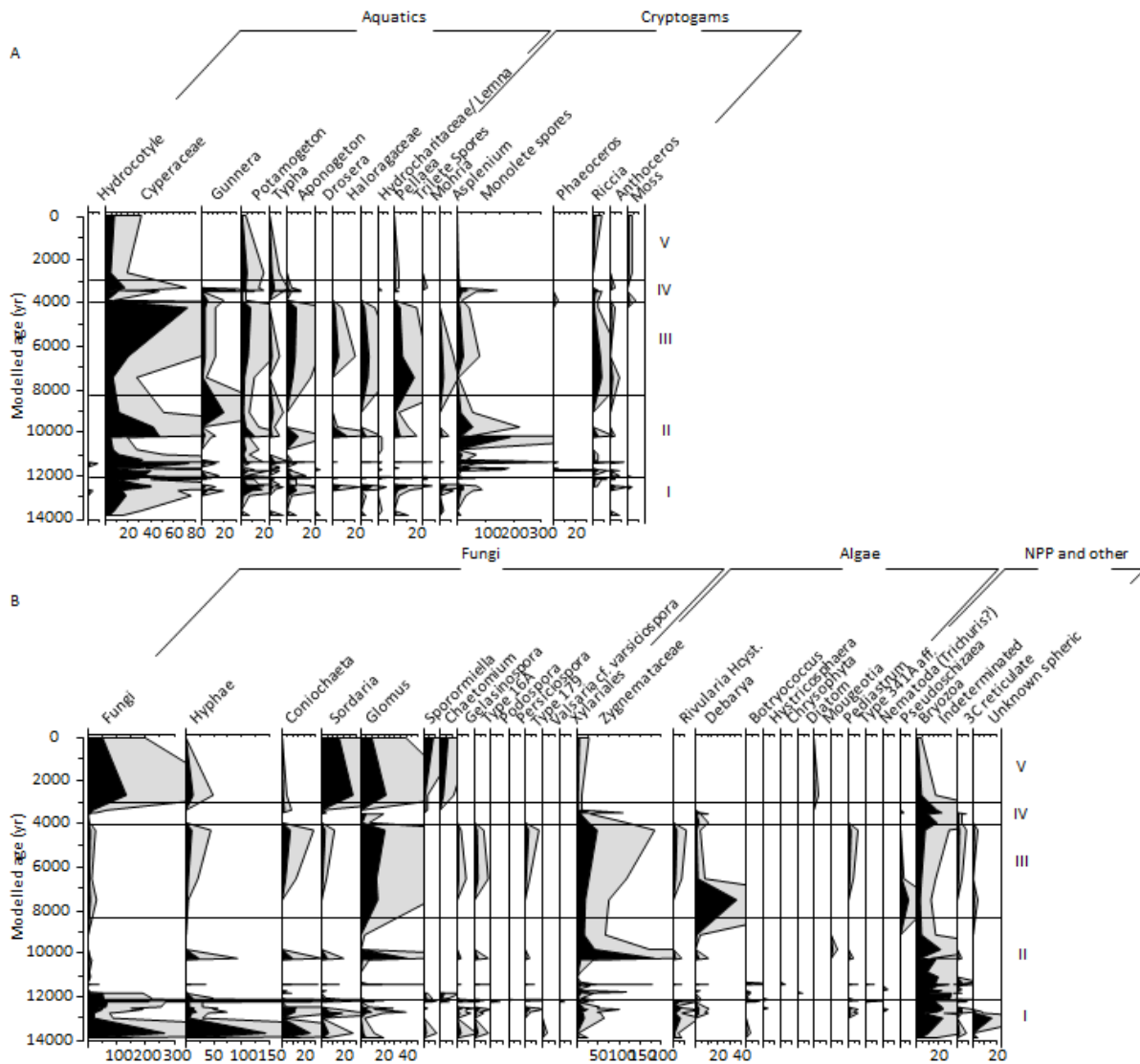
362

363

364

365

Fig. 9. A. Arboreal, fynbos and Asteraceae pollen. B pioneer, other non-arboreal and succulent pollen. Zones on the right in B are determined by the CONISS cluster diagram based on taxa represented in both A and B.



366

367 Fig. 10. Aquatic pollen, cryptogam spores and NPP's. Pollen zones on the right are based on  
 368 the regional taxa in Fig. 9.

369

370 The diagrams of arboreal and non-arboreal pollen show sharp relatively short-term  
 371 oscillations, but long-term or developmental trends are difficult to visualise. The zonation is  
 372 therefore based on the CONISS results: I) 13.9- 2.1 ka, II) 12.1-8.3 ka, III) 8.5- 4 ka, IV) 4-3 ka  
 373 and V) 3 ka-present (Fig. 9B).

374

375           Pollen zone I (13.9-12.1 ka) starts with prominent Asteraceae (undifferentiated) peak  
376 accompanied by an initial prominence of *Stoebe* type at 13.9 ka. It is otherwise associated  
377 mainly with grasses (Poaceae), some trees (*Euclea* sp.) and some fynbos shrubs (Ericaceae,  
378 *Passerina* sp. and Restionaceae). The Younger Dryas (YD) period (c. 12.8-11.5 ka) spans the  
379 transition between Pollen zones I and II (12.1-8.3 ka). Pollen from the base of the YD (Pollen  
380 zone I) continues to show relatively high proportions of Asteraceae (undifferentiated), while  
381 some woody plant pollen like *Euclea*, *Clutia* and *Buddleja* increase, together with  
382 Restionaceae and some fynbos elements. The woody elements decline c. 11.7 ka and some  
383 of the fynbos, e.g., Ericaceae, *Passerina* sp. and *Cliffortia* sp. continues to be present in fair  
384 numbers in Pollen zone II (Fig. 9 A). Grass and Asteraceae pollen (including varying numbers  
385 of *Stoebe* type) are prominent while different fynbos types persist. Of the fynbos types,  
386 Restionaceae pollen shows a strong decline c. 11 ka, after which succulents (Aizoaceae type  
387 and *Ruschia*) peak c. 10.1 ka followed by a moderate return of Restionaceae pollen. This  
388 followed at the top of Pollen zone II (c. 9 ka), by a marked grass pollen increase.

389 Pollen zone III (8.5-4 ka) has lower resolution due to poor pollen preservation, but shows  
390 more grass and Asteraceae, including *Stoebe* type (probably including *Elytropappus*) up to  
391 about 6.5 ka when succulents like Aizoaceae and *Crassula*-type become prominent. Pollen  
392 zone IV (4-3 ka) at c. 3.8 ka shows prominent grasses, Asteraceae and eventually Restionaceae  
393 pollen and in a relatively short section up to c. 3.3 ka, although there is considerable variation  
394 in pollen composition. At c. 3.5-3.4 ka, types like *Morella* peak while others e.g., *Euclea* and  
395 *Stoebe* type, decline. The top section (Pollen zone V, 3 ka to the present) representing brown  
396 sands, is poorly covered as result of insufficient pollen preservation, but the available level at  
397 c. 2.6 ka is similar to the modern spectrum (Fig. 9).

398

## 399 5. Discussion

400 Transport of material from the higher ground probably influenced the different  
401 proxies. For instance, where karroid, succulent or grassy elements in the deposits occur, they  
402 probably reflect changing conditions in the source area within the uplands to the south, which  
403 is now under fynbos. This, via the presence of C<sub>4</sub> or CAM plants, may account for the varying  
404 composition of accompanying organic matter, phytoliths and pollen, and other inclusions  
405 from the surrounding slopes. Changes in rainfall seasonality, stream energy, etc., would also  
406 affect this. Mixed with the transported material are potentially the remains of local elements  
407 at the study site typical of the drainage course.

408

### 409 5.1. Geochemistry interpretation

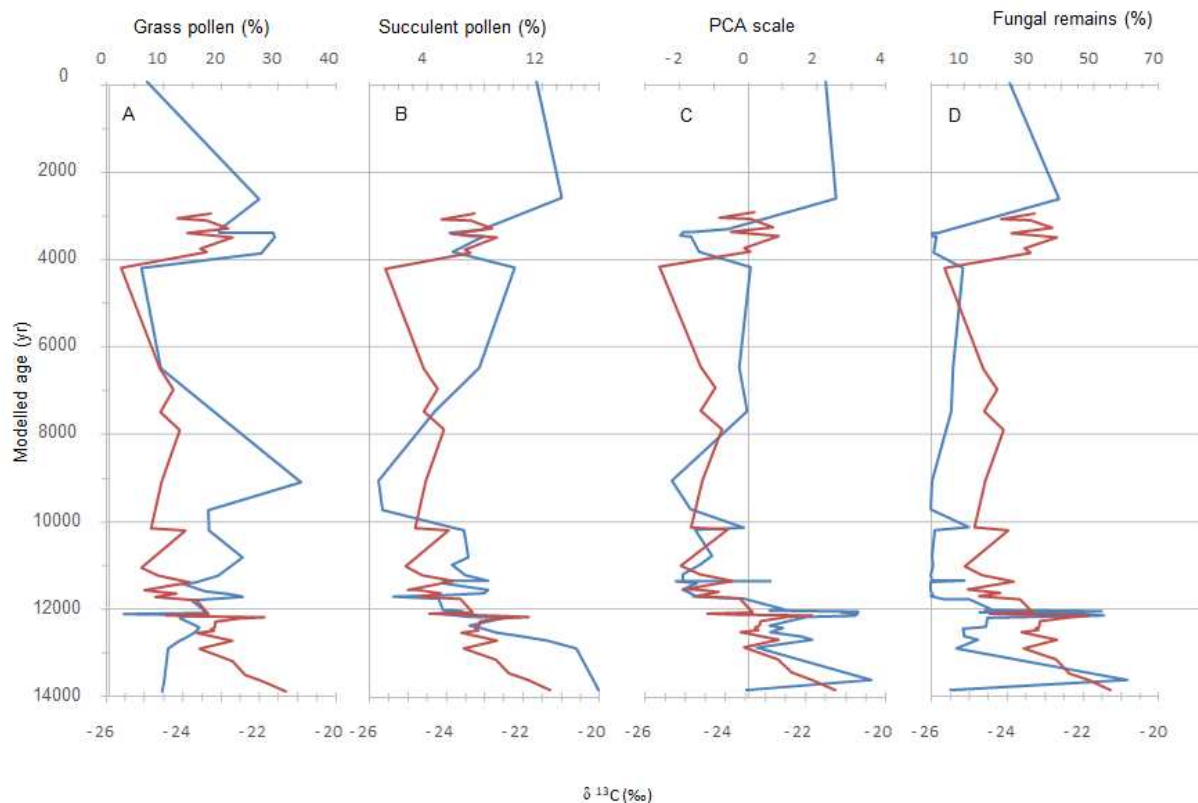
410 The highly variable TOC content of the sediments largely reflects the varied  
411 depositional environment, with high TOC associated with fine grain sedimentary units, most  
412 likely overbank fines, waning limbs of flood events or palaeo-landsurfaces, and low TOC  
413 associated with flood deposits of coarse-grained sands and gravels. The former are  
414 particularly associated with the phase of relatively fast valley fill aggradation ~14-10 ka. The  
415 largely invariant TOC/TN ratios of 15-25 are typical of the measured range of Fynbos and  
416 Succulent Karoo Biome soils (Carr et al. 2013) (Fig. 4B), consistent with a largely terrestrial  
417 organic matter sediment source throughout the sequence. The lowest values of  $\delta^{13}\text{C}_{\text{TOC}}$  are  
418 consistent with contributions from C<sub>3</sub> vegetation (global mean C<sub>3</sub>  $\delta^{13}\text{C}$  -26 ‰; O'Leary et al.,  
419 1988; Diefendorf et al., 2010) (Fig. 4C, blue shading), and such values are characteristic of  
420 fynbos vegetation (Vogel et al., 1978; Carr et al., 2016). The higher  $\delta^{13}\text{C}_{\text{TOC}}$  values (> -22 ‰)  
421 imply some contribution from non-C<sub>3</sub> vegetation, potentially including C<sub>4</sub> grasses ( $\delta^{13}\text{C}$   
422 typically -10 to -14 ‰; O'Leary et al., 1988) or CAM plants ( $\delta^{13}\text{C}$  highly variable but high as -

423 12 ‰; Rundel et al., 1999). Soils (Fig. 4C, pink shading) in the Succulent Karoo biome, to which  
424 CAM plants may variably contribute organic matter, typically have  $\delta^{13}\text{C}_{\text{TOC}}$  values of -22 to -23  
425 ‰ (Carr et al., in prep). Soils in the Nama Karoo, for which  $\text{C}_4$  grasses may contribute organic  
426 matter typically have  $\delta^{13}\text{C}_{\text{TOC}}$  ranging between -22 and -14 ‰, depending on grass  
427 cover/summer rainfall amount (Bond et al., 1994).

428

429 For the KMR record overall there is no correlation between  $\delta^{13}\text{C}_{\text{TOC}}$  and grass pollen  
430 (Fig. 11A), but both  $\text{C}_3$  and  $\text{C}_4$  grasses were present based on the phytolith evidence (e.g., at  
431 c. 9ka; Fig. 7, Fig. 12), and the latter parts of the record (e.g. 6-3 ka) show some potential  
432 correlation with grass pollen abundance, if not the phytolith-derived  $\text{C}_3/\text{C}_4$  ratio. Other  
433 correlations between the isotope and pollen data are identified. The sum of the succulent  
434 pollen types (Fig. 11 B) correlates with  $\delta^{13}\text{C}_{\text{TOC}}$  ( $r=0.37$   $p=0.04$  for the whole record and more  
435 strongly ( $0.43$ ,  $p = 0.04$ ) for the section 14-9 ka (Fig. 11C, S6B/&b). Thus, one interpretation  
436 of the isotope data is that a varying proportion of CAM plants (succulents) contributed to the  
437 soil organic matter of the KMR catchment (Fig. 11B). As CAM physiology is essentially an  
438 adaptation to drought, this would imply that during periods of greater aridity there were  
439 greater inputs of CAM-plant derived organic matter from the catchment soils.

440



441

442 Fig. 11. A. Loess smoothed grass (blue) and  $\delta^{13}\text{C}_{\text{TOC}}$  (red). B. Slightly Loess smoothed summed  
 443 succulents (blue) and  $\delta^{13}\text{C}_{\text{TOC}}$  (red). C. Local pollen & spore PCA axis 1 vs.  $\delta^{13}\text{C}_{\text{TOC}}$ . D. Fungi %  
 444 vs.  $\delta^{13}\text{C}_{\text{TOC}}$

445 However, considering the  $\delta^{13}\text{C}_{\text{TOC}}$  data in relation to the local pollen-fungal elements  
 446 PCA axis 1 we also observe a correlation between these elements and  $\delta^{13}\text{C}_{\text{TOC}}$  (Fig. 11C) (see  
 447 Supplemental Material, Fig. S6B/7B. This reflects a positive (negative) correlation between  
 448  $\delta^{13}\text{C}_{\text{TOC}}$  and fungal spores (local vegetation elements). The overall correlation with axis 1 is  $r =$   
 449  $0.50$  ( $p = 0.006$ ), with the correlation stronger for samples older than 10 ka ( $r = 0.61$ ;  $p = 0.004$ )  
 450 (Fig. 11C and D). The implied decreasing  $\delta^{13}\text{C}_{\text{TOC}}$  in association with increased  
 451 local/riparian/aquatic pollen inputs could therefore also reflect a shift in the sources of the  
 452 organic matter input to the sediments; i.e. from a wider catchment contribution that includes  
 453 CAM and soil fungi inputs to a dominantly local  $\text{C}_3$  riparian / wetland vegetation input, with

454 the latter occurring as the land-surface in the channel stabilised and was colonised by  
455 vegetation (also accounting for the accompanying increased TOC).

456

## 457 *5.2. Vegetation conditions and trends*

458 Here we summarize all proxies according to arbitrary time zones as phytolith and  
459 palynological zonations (Figs. 6-8 and Figs. 8-10) correspond broadly, but are not identical.

460

461 In 14-10.5 ka (8.9–4.5 m), predominantly organic-rich, layers of sand show high but  
462 steadily declining  $\delta^{13}\text{C}_{\text{TOC}}$  values (except for a spike a spike within YD times at c. 12.2 ka (Fig.  
463 4C), associated with increasing TOC. The proportions of Poaceae phytoliths, of which the  
464 majority are  $\text{C}_3$  grasses, increase during this phase. The phytolith data provide further clues  
465 for the vegetation reconstruction ancillary to the pollen data, particularly for the graminoids.  
466 In the phytolith assemblage of 13.7-12.9 ka, the high incidence of non-graminoids (woody and  
467 shrubby vegetation), abundant Restionaceae and relatively low proportions of Poaceae imply  
468 a dominance of fynbos vegetation (Cordova, 2013; Cordova and Avery, 2017). Distinctively,  
469 the burnt grass phytoliths count is lower. However, despite the limited Poaceae, there is an  
470 important incidence of  $\text{C}_3$  grasses, suggesting some winter season rains. The relative  
471 importance of Chloridoideae suggests either occasional dryness or diminished summer rain.

472

473 The higher incidence of Poaceae over Restionaceae and the lower proportions of non-  
474 graminoids c. 12.9-10.6 ka suggest a grassier environment, still within a matrix of Ericaceous  
475 fynbos. This could be a type of grassy fynbos like the ones found farther east (cf. Rebelo et  
476 al., 2006) or the amplification of the renosterveld (*Stoebe* type), which normally has more  
477 grasses (Cordova, 2013; Cordova and Avery, 2017). However, given the incidence of

478 Panicoideae, it is possible that increased summer rain prompted more lightning-initiated fires,  
479 as it currently occurs in areas of fynbos farther east, thus promoting the spread of grasses and  
480 the decline of Ericaceae and Thymeleaceae. The pollen data further suggest grassy karroid  
481 vegetation, which probably included *Elyropappus* (*Stoebe* type), with some fynbos elements,  
482 especially Restionaceae, and decreasing succulent abundance. The latter may explain the high  
483 but declining  $\delta^{13}\text{C}_{\text{TOC}}$  through this period, although this reduction in  $\delta^{13}\text{C}_{\text{TOC}}$  may also reflect  
484 the aforementioned increased organic matter inputs from local aquatic ( $\text{C}_3$ ) vegetation, which  
485 also peak  $\sim 11$  ka. Both the burned phytoliths and the charcoal suggest increased burning  $\sim 12$   
486 ka within the YD phase.

487

488 The period 10.5-7 ka (4.5-3.3 m) is associated with a much-reduced sample resolution  
489 and some gravel inclusions that probably experienced erosion. It consists otherwise of grey  
490 to black organic sands, rich in TOC up to 10 ka, but declining from c. 9 ka, with relatively low  
491  $\delta^{13}\text{C}_{\text{TOC}}$  (likely  $\text{C}_3$  vegetation derived) (Figs. 4 and 13). At around 10 ka, there is a brief peak of  
492 montane woodland pollen, e.g., *Podocarpus*, *Clutia*, *Buddleja* and *Euclea* together with fynbos  
493 (Fig. 9A). Next during this phase, high percentages of grass phytoliths and grass pollen occur  
494 at c. 9 ka. Judging from the isotope and phytolith composition the parent plants were  
495 predominantly  $\text{C}_3$  grasses, but  $\text{C}_4$  grasses were also present (Fig. 7, 12), which occurred  
496 together with Restionaceae, undifferentiated Asteraceae and *Stoebe* type (probably, also  
497 including *Elytropappus*) (Figs.9A).

498

499 The sandy section, 7 ka-4.1 ka (3.3-2.9 m), associated with relatively low TOC contents  
500 (Fig. 4A) accumulated relatively slowly and preserves few pollen and phytoliths, possibly due  
501 to exposure and drying. It shows relatively low  $\delta^{13}\text{C}_{\text{TOC}}$  values c. 7-6.5 ka (sequence minimum



502 value of -25.6 ‰ at c. 4.2 ka) (Fig. 4C). The absolute values in both periods suggest dominantly  
503 C<sub>3</sub> vegetation inputs, although there is marginally higher  $\delta^{13}\text{C}_{\text{TOC}}$  at 7-6.5 ka, coeval with a  
504 single phytolith level (6.5 ka) (Fig. 7) that indicates an increased C<sub>4</sub> grass component. Around  
505 6.5 ka we observe an increase in succulent pollen together with other mountain slope  
506 vegetation like Ericaceae, *Euclea* and *Clusia*. The proportions of phytolith assemblages and  
507 GSSC distribution prior to c. 6.0 ka provide limited information, although it is possible that  
508 rainfall was equally spread during summer and winter. After 6.0 ka there is a reduction in  
509 woody/shrubby vegetation and an apparent increase in Chloridoideae, which may reflect dry  
510 conditions similar to the Succulent Karoo, where Chloridoideae grasses tend to dominate  
511 (Cordova and Scott 2010; Cordova 2013).

512

513         The section, 4.1-2.6 ka (1.9-0.6 m), starts with an iron stained orange sand covered by  
514 grey sands. The TOC content varies but is generally low except for some darker grey horizons  
515 and  $\delta^{13}\text{C}_{\text{TOC}}$  increases to values more akin to those of the late Pleistocene (-23.5 ‰) . The  
516 phytolith assemblages suggest the expansion of fynbos, but unlike the period c. 12.9-10.6 ka,  
517 this fynbos has a higher incidence of grasses, with evidence for frequent burning (Figure 6).  
518 Grass phytoliths are mainly of the C<sub>3</sub> type with little C<sub>4</sub> representation, but a variable to strong  
519 succulent presence in the pollen data may account for the  $\delta^{13}\text{C}_{\text{TOC}}$  trend. Typical woody slope  
520 elements, Asteraceae and fynbos, including Restionaceae are present, especially at c. 3.4 ka.  
521 It is possible that winter rains were dominant, but at times summer rains must have occurred,  
522 perhaps even more than today.

523

524 The brownish upper sands, 2.6-0 ka (0.6m-0m), do not preserve pollen and phytoliths.  
525 However, the modern surface sample shows a strong presence of Poaceae phytolith  
526 morphotypes with some C<sub>4</sub> grass representation, Asteraceae and succulent pollen.

527

### 528 5.3. General synthesis of environmental changes of the KMR sequence

529 The opposing dynamics between Poaceae and Asteraceae and other fynbos and  
530 succulent taxa observed in the KMR sequence are not reflected in the modern pollen transect  
531 (Fig. S5). This is, however, not unexpected as in the modern transect the higher grass  
532 proportions towards the karroid vegetation to the north, represent mostly C<sub>4</sub> grass (cf.  
533 Cordova and Avery 2017, their Figs. 5a and 8), while we have phytolith evidence that the grass  
534 peaks in the fossil sequence largely represent C<sub>3</sub> grass. The question then arises as to what  
535 conditions the combination of C<sub>3</sub> grasses and Asteraceae observed at 9 ka in the KMR would  
536 imply (Fig. 9, Fig. S6A and S7A). If it represented a cool, relatively dry environment with winter  
537 growth, this would find support in the (low)  $\delta^{13}\text{C}_{\text{TOC}}$  values. After 8 ka some C<sub>4</sub> grasses occur,  
538 but with only slightly increased isotope values. The  $\delta^{13}\text{C}_{\text{TOC}}$  decreases before 4 ka, at a time  
539 when fynbos including Ericaceae, Restionaceae and *Stoebe* type, probably including  
540 *Elytropappus* (renosterbos), is observed to increase in the pollen spectra. This vegetation  
541 suggests relatively moist conditions.

542 Alternations of aquatic pollen types, cryptogam spores, fungal spores and algae can  
543 be related to interaction between flooding events, stream energy, stream transport, fungal  
544 decay and selective preservation. There are marked trends in the occurrence of fungal  
545 remains through the sequence. For the period 14-11 ka there are elevated, albeit declining  
546 fungal elements (Fig. 11D) and initially reduced local wetland, cryptogamic and algal  
547 elements, which become increasingly abundant towards 11 ka. Indeed, during this phase

548 there is a correlation between fungal elements and the  $\delta^{13}\text{C}_{\text{TOC}}$ , under otherwise cool, dry and  
549 relatively stable conditions, while according to the phytoliths, a transition to more  $\text{C}_3$   
550 vegetation took place and fungal remains declined. The process was gradual except for a brief  
551 reversal during YD times. This is also a period associated with steady accumulation of the  
552 sediment sequence (i.e. aggradation of the fluvial system), possibly transporting soil fungi  
553 from the surrounding slopes, although it is not possible to determine how much was  
554 transported or locally produced. Fungal remains in the deposits subsequently decline in  
555 favour of active local plant and algal growth up to around 4-3 ka (Fig. 11 D) (PC 1, Fig. 11 C,  
556 see also Fig. S6B/S7B) where there is a shift in  $\delta^{13}\text{C}_{\text{TOC}}$  that coincides with increased succulent  
557 pollen, potentially implying increased CAM or  $\text{C}_4$  vegetation contributions. The return of  
558 fungal remains is, however, delayed until 2.6 ka when drier conditions set in and there is a  
559 more prominent appearance of succulent Aizoaceae type pollen (Fig. 11 B). The increase in  
560 fungal remains can either be attributed to the more stable soil formation processes at the site  
561 itself or to transport of soil material from the surrounding slopes, or both.

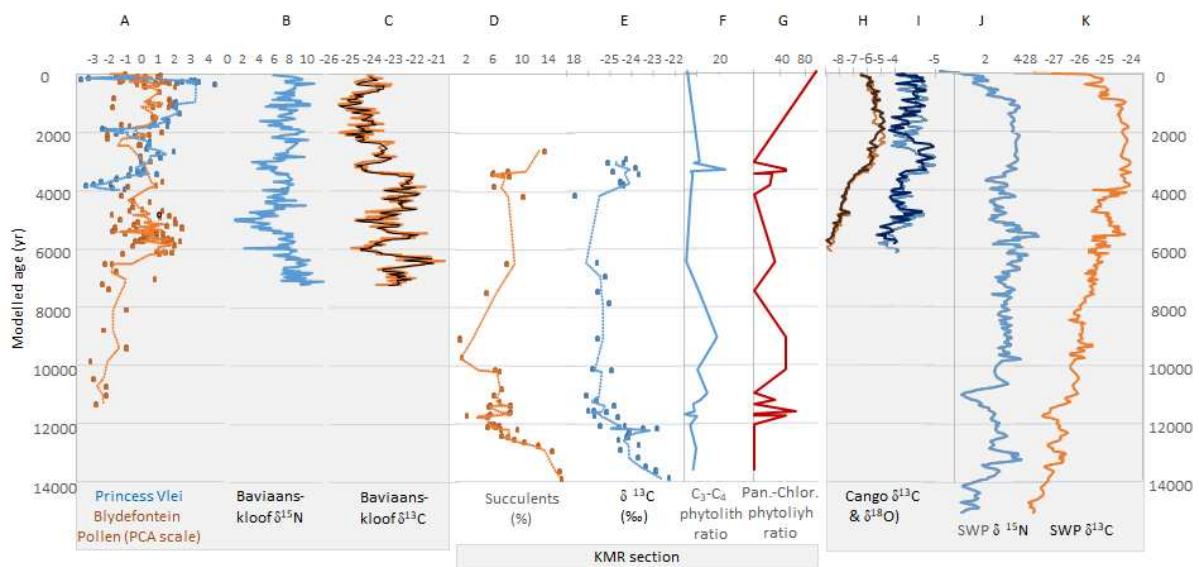
562

#### 563 *5.4. Regional comparisons*

564 The KMR sequence provides several lines of evidence potentially indicative of changes  
565 in rainfall amount and seasonality. The findings can be placed in a wider context to  
566 reconstruct a regional history through comparison with other proxy sequences (Fig. 12).  
567 Notably, the nearest palaeoenvironmental record is the Baviaanskloof Rock hyrax midden  
568 record ~50 km to east. This provides evidence for vegetation ( $\delta^{13}\text{C}$ ) and climatic ( $\delta^{15}\text{N}$ )  
569 changes over the last 7 ka (Chase et al. 2020) (Fig. 12B & C). ~80 km to the west of KMR, the  
570 Cango Cave stalagmite record provides temperature ( $\delta^{18}\text{O}$ ) and vegetation ( $\delta^{13}\text{C}$ ) proxies  
571 spanning the last 6 ka (Talma and Vogel, 1992) (Fig. 12A). Cango Cave lies close to the

572 Boomplaas Cave archaeological site, for which a recent reconstruction of rainfall seasonality  
 573 and rainfall amount has been presented using micromammal evidence (Faith et al., 2018),  
 574 while 150 km to the west, the longer hyrax dung sequence from Seweweekspoort (Fig. 12J,  
 575 K) (Chase et al., 2013; 2018) provides both isotope and pollen evidence from marine isotope  
 576 stage 2 to the present.

577



578

579 Fig. 12. The KMR section with various proxies from the Western and Eastern Cape Provinces  
 580 (numbers in brackets below refer to positions in Fig. 1A.). A. Pollen PCs Blydefontein (7)  
 581 (brown) (Scott et al., 2012, chronology adjusted) and Princess Vlei (14) (blue) (Neumann et  
 582 al., 2011; Cordova et al., 2019), B. Baviaanskloof (8),  $\delta^{15}\text{N}$  ‰, C.  $\delta^{13}\text{C}$  ‰ (Chase et al., 2020),  
 583 D. KMR, Succulent pollen %, E. KMR  $\delta^{13}\text{C}_{\text{TOC}}$  ‰, F. KMR  $\text{C}_3/\text{C}_4$  phytolith ratio, G. KMR  
 584 Panicoideae/Chloridoideae phytolith ratio (this study), H. Cango Caves (9):  $\delta^{13}\text{C}$  ‰, I.  $\delta^{18}\text{O}$  ‰  
 585 (solid lines Talma and Vogel, 1992, faded lines Chase et al., 2013 chronology), J.  
 586 Seweweekspoort (10) J.  $\delta^{15}\text{N}$  ‰, K.  $\delta^{13}\text{C}$  ‰ (Chase et al., 2013, 2018).

587

588           In KMR, the dominantly present C<sub>3</sub> grass phytoliths (with C<sub>4</sub> present, but never  
589 dominant), the high incidence of non-graminoids (woody and shrubby vegetation) and the  
590 abundant Restionaceae observed 14-10.5 ka are not inconsistent with recent reconstructions  
591 of a relatively humid, mixed summer-winter rainfall environment for the latest Pleistocene  
592 (i.e. last glacial-interglacial transition) (Chase et al., 2018; Faith et al., 2018). The trend in  
593  $\delta^{13}\text{C}_{\text{TOC}}$  and succulent pollen at KMR during this phase (both peaking at 14 ka and potentially  
594 implying some aridity), presents potential evidence for variability around this scenario  
595 (indeed, it is opposed to the overall increasing trend in  $\delta^{13}\text{C}$  seen in the SWP record (Fig. 12)  
596 (Chase et al., 2018). However, the Seweweekspoort  $\delta^{15}\text{N}$  record (Chase et al., 2018) indicates  
597 short-term variability in water availability within the 15-10 ka period, with a trend from  
598 relatively arid to relatively wetter conditions ~13.3-11 ka (Fig. 12) that is perhaps consistent  
599 with observations at KMR, including the reduction in succulent pollen observed during this  
600 period. Based on the Boomplaas micromammal record, Faith et al. (2018) presented a  
601 reconstruction for the Pleistocene-Holocene transition that indicated increasing winter  
602 rainfall contributions from ~13-10 ka, associated with a trend towards relatively arid  
603 conditions. Consistent with this, at KMR the phytolith data show a steady reduction in the  
604 C<sub>4</sub>/C<sub>3</sub> ratio to a minimum at ~10 ka. Additionally, by 9 ka, relatively more C<sub>3</sub> grasses developed  
605 (Fig. 7, 12F) in a grassier, more frequently burned environment with a higher incidence of  
606 Poaceae over Restionaceae and lower proportions of non-graminoids c. 12.9-10.6 ka and at 9  
607 ka. The precession cycle (Berger and Loutre, 1991) would have promoted winter rainfall at  
608 around 9 ka (Street-Perrott and Perrott, 1993; Partridge et al., 1997).

609           Given the low sampling resolution for the early to mid-Holocene, detailed  
610 comparisons are challenging, especially c. 4-7 ka when there seems to be much variability in  
611 several records, notably the sharp c. 5 ka negative (increased humidity) deviation in  $\delta^{15}\text{N}$  at

612 Baviaanskloof (Chase et al. 2020). By 6.5 ka precessional forcing in this all-year seasonality  
613 zone would probably favoured slightly more summer rains, but moderately dry conditions  
614 with succulents and Asteraceae persisted, with some C<sub>4</sub> grass (more apparent from phytoliths  
615 than isotope values).

616         The resolution at KMR is too poor to draw conclusions as to the effects of the  
617 maximum sea ice extent in the South Atlantic at ~4.3 ka (Nielsen et al., 2004). However, the  
618 period 4-2 ka offers an opportunity for comparison with several records. Here KMR record  
619 shows a  $\delta^{13}\text{C}_{\text{TOC}}$  minimum (-25.6 ‰) at or prior to ~ 4.2 ka and then stabilises at ~-23‰ from  
620 3.7-3.1 ka. This transition is associated with relatively grassy fynbos vegetation, increased  
621 succulent pollen and increased evidence of burning. The Cango Cave speleothem (Talma and  
622 Vogel, 1992) exhibits an increase in  $\delta^{13}\text{C}$  starting at 3 ka and peaking by c. 2 ka (Fig. 12I).  
623 However, Chase et al. (2013) suggest a revised chronology that places this peak at c. 3 ka. The  
624 SWP midden, which also exhibits its highest grass pollen concentrations at this time, has high  
625  $\delta^{13}\text{C}$  values between 3 and 1 ka (Fig. 12K) (Chase et al., 2018). These observations are  
626 consistent with the increased abundance of grass pollen and phytoliths at KMR c. 3 ka, where  
627 interestingly (for interpretation of  $\delta^{13}\text{C}$  trends) the phytolith data suggest this was largely C<sub>3</sub>  
628 grass with lower amounts of C<sub>4</sub> types (Fig. 12D-G). At Cango the associated  $\delta^{18}\text{O}$  temperature  
629 record indicates a relatively sharp 1°C increase at about <2ka (Talma and Vogel, 1992; Fig.  
630 12H) but Chase et al. (2013) suggest that this occurred at about 3 ka. At the same time the  
631 Baviaanskloof midden also shows a marked change in  $\delta^{13}\text{C}$  and  $\delta^{15}\text{N}$ , although the direction  
632 of the former proxy (a shift to lower  $\delta^{13}\text{C}$ ) is opposite to that observed at SWP and Cango  
633 Caves (i.e. it is reduced, implying more C<sub>3</sub> vegetation consumption by the hyraxes, perhaps  
634 dependent on their dietary preferences for available plant species). Overall however, the  
635 year-round rainfall zone exhibits consistent evidence for a marked climatic/ecological

636 transition at this time, presumably in response to increased temperatures (Talma and Vogel,  
637 1992; Chase et al., 2013). Whether such increased temperature was associated with reduced  
638 winter rainfall/increased summer rainfall (see Chase et al., 2017, 2018) is less clear given the  
639 apparently limited response in the KMR phytolith data and the contrasting  $\delta^{13}\text{C}$  trajectories  
640 in the hyrax midden records. Indeed, the increase in succulent pollen at KMR is consistent  
641 with reduced moisture availability (i.e. aridity) associated with such a temperature increase,  
642 as might be the reduced palatability/availability (for hyraxes) of ( $\text{C}_4$ ) grasses (Chase et al.,  
643 2020). Considering regional climatic drivers, the KMR sequence can be viewed in terms of the  
644 hypothesis of Chase and Quick (2018), which emphasises the role of the warm Agulhas current  
645 in driving climatic variability in the southern coastal region, in direct contrast to drivers and  
646 trends in the nearby southern interior areas. The Seweweekspoort record c. 80 km from the  
647 coast (Chase et al., 2017, Chase and Quick, 2018) provided evidence to support this  
648 hypothesis, while the Baviaanskloof record, if differing in detail, provides some further  
649 support for this coastal-interior dichotomy. In this sense comparisons between these interior  
650 sites and KMR broadly provide support this model (in general if not perhaps in terms of details  
651 at smaller temporal scales).

652         Deeper inland from KMR, ~ 330 km to the northeast, is the Blydefontein site in the  
653 summer rain region of the Nama Karoo Biome (Mucina and Rutherford, 2006). Here the  
654 Holocene pollen record provides evidence of moisture availability based on grass cover versus  
655 karroid shrub cover (Scott et al., 2005, 2012, 2020). After a humid spell between 6 and 4.5 ka  
656 it suggests relative dryness, probably a decline in summer rain, occurred just before 4 ka at  
657 the time when at KMR succulents, renosterbos (*Stoebe* type), other Asteraceae and Ericaceae  
658 were prominent and grasses were reduced. The change to wetter conditions that follows,  
659 suggest a regional climatic coherence between Blydefontein and KMR in terms of moisture

660 availability for the time between c. 4.2 ka and 3 ka. Both seem to follow the interior pattern  
661 that is also inferred at the Cango Cave and Seweweekspoort (Chase et al., 2013, 2020; Chase  
662 and Quick, 2018). This is not the case in the coastal area at Eilandvlei (Quick et al., 2018) and  
663 Still Bay (Quick et al., 2015), where a decline in afro-temperate forest is evident just before 4  
664 ka, or at Princess Vlei further to the west where pollen suggest relatively dry conditions (Fig.  
665 12) at this time (Neumann et al., 2011; Cordova et al., 2019). The pattern of climate  
666 development at KMR sequence therefore seems to conform to that in the interior rather than  
667 the coastal pattern, as proposed by Chase and Quick (2018), even if it is only about 40 km  
668 from the coast.

669

## 670 **6. Conclusions**

671 The Holocene KMR section provides the first multi-proxy study of palaeoenvironments  
672 as derived from an alluvial sequence in the relatively dry all-year rainfall zone in the Western  
673 and Eastern Cape border area. It demonstrates how the different proxies complement each  
674 other and contribute to our understanding of changing conditions in a complex depositional  
675 system. The sequence of deposits starts shortly before the Northern Hemisphere's Younger  
676 Dryas event. At this time we observe relatively fast accumulation of deposits under dry  
677 conditions. Together the lithology, isotope, phytolith and pollen data suggest a shift towards  
678 alternating phases of humid and dry events with higher stream energy, slower accumulation  
679 and subtly changing seasonality during the early and middle Holocene, as far as can be  
680 ascertained from the relatively low sample resolution. By c. 4 ka a relatively humid phase  
681 started after which pollen and phytolith preservation in the upper layers became poor,  
682 presumably due to drier conditions.



683           In terms of regional forcing, the results suggest that the climatic development at KMR  
684 during the Holocene, a location only c. 40 km from the coast, despite minor short-term  
685 deviations, conforms more to patterns identified in the interior Karoo region than to those  
686 observed in peri-coastal sites. To further investigate the geographic scope of coastal Agulhas  
687 Current climate forcing, a similar set of deposits of the same age has been located further to  
688 the south (Louterwater, in the Langkloof, c. 30 km from the coast), which will allow us to test  
689 this hypothesis in further studies.

690 Supplementary Material (link here).

691

## 692 **Acknowledgements**

693           We thank Peter Holmes, who accompanied us to the studied site and coined the term  
694 KMR based on the Kamanassie River. Martin Wessels and Maitland Seaman assisted with  
695 fieldwork and photography. Andri van Aardt is thanked for laboratory and travel  
696 arrangements. LS was supported by the National Research foundation (South Africa) (NRF  
697 Grant no. 85903). SM was supported by the NRF Competitive Programme for Rated  
698 Researchers (118538) and a travel grant from the Ministry of Economy and Competitiveness  
699 (Spain) and JO and JSC by Project CGL-PID2019-1049449GB-I00 (FEDER/Ministry of Science  
700 and Innovation, Spain). ASC's contribution was supported by the Leverhulme Trust (Grant  
701 F/00 212/AF).

702

## 703 **References**

704 Berger, A., Loutre, M.F., 1991. Insolation values for the climate of the last 10 million years.  
705 Quaternary Sciences Review 10, 297-317.

- 706 Blaauw, M., Christen, J. A., 2011. Flexible paleoclimate age-depth models using an  
707 autoregressive gamma process. *Bayesian Analysis* 6, 457–474.
- 708 Bond, W.J., Stock, W.D., Hoffman, M.T. 1994. Has the Karoo spread? A test for desertification  
709 using carbon isotopes from soils. *South African Journal of Science* 90, 391-397.
- 710 Bousman, C.B., Partridge, T.C., Scott, L., Metcalfe, S.E., Vogel, J.C., Seaman, M., Brink, J.S.  
711 1988. Palaeoenvironmental implications of Late Pleistocene and Holocene valley fills in  
712 Blydefontein basin, Noupoot, C.P., South Africa. *Palaeoecology of Africa* 19, 43-67.
- 713 Carr, A.S., Boom, A., Chase, B.M., Meadows, M.E., Roberts, Z.E. Britton, M.N., Cumming,  
714 A.M.J. 2013. Biome-scale characterisation and differentiation of semi-arid and arid zone soil  
715 organic matter compositions using pyrolysis-GC/MS analysis. *Geoderma* 200-201, 189 – 201.
- 716 Carr, A.S., Chase, B.M., Boom, A., Medina-Sanchez, J. 2016. Stable isotope analyses of rock  
717 hyrax faecal pellets, hyraceum and associated vegetation in southern Africa: implications for  
718 dietary ecology and palaeoenvironmental reconstructions. *Journal of Arid Environments* 134,  
719 33-48.
- 720 Carr, A.S., Chase, B.M., Boom, A., Meadows, M.E. Soil and foliar stable carbon and nitrogen  
721 isotope compositions in the Fynbos and Succulent Karoo Biomes. In prep.
- 722 Chase B.M., Meadows M.E. 2007. Late Quaternary dynamics of southern Africa's winter  
723 rainfall zone. *Earth Sci Rev* 84, 103-138.
- 724 Chase, B.M., Boom, A., Carr, A.S., Meadows, M.E., Reimer, P.J. 2013. Holocene climate change  
725 in southernmost South Africa: rock hyrax middens record shifts in the southern westerlies.  
726 *Quaternary Science Reviews* 82, 199–205.
- 727 Chase, B.M., Lim, S. Chevalier, M., Boom, A., Carr, A.S., Meadows M.E., Reimer, P. J. 2015.  
728 Influence of tropical easterlies in southern Africa's winter rainfall zone during the Holocene.  
729 *Quaternary Science Reviews* 107, 138-148.

- 730 Chase, B.M., Chevalier, M., Boom, A., Carr, A.S. 2017. The dynamic relationship between  
731 temperate and tropical circulation systems across South Africa since the Last Glacial  
732 Maximum. *Quaternary Science Reviews* 174, 54-62.
- 733 Chase, B.M., Faith, J.T, Mackay, A., Chevalier, M., Carr, A.S., Boom, A., Lim, S., Reimer, P.J.  
734 2018. Climatic controls on Later Stone Age human adaptation in Africa's southern Cape.  
735 *Journal of Human Evolution* 114, 36-45.
- 736 Chase, B.M. and Quick, L 2018. Influence of Agulhas forcing of Holocene climate change in  
737 South Africa's southern Cape. *Quaternary Research* 2018, 1-7.
- 738 Chase, B.M., Boom, A., Carr, A.S. Quick, L.J, Reimer, P.J. 2020. High-resolution record of  
739 Holocene climate change dynamics from southern Africa's temperate-tropical boundary,  
740 Baviaanskloof, South Africa. *Palaeogeography, Palaeoclimatology, Palaeoecology* 539,  
741 109518.
- 742 Chevalier, M., Chase, B.M., 2015. Southeast African records reveal a coherent shift from high-  
743 to low-latitude forcing mechanisms along the east African margin across last glacial-  
744 interglacial transition. *Quat. Sci. Rev.* 125, 117-130.
- 745 Cohen, T. J., Nanson G. C. 2007. Mind the gap: An absence of valley-fill deposits identifying  
746 the Holocene hypsithermal period of enhanced flow regime in southeastern Australia. *The*  
747 *Holocene* 17(3), 411-418.
- 748 Cordova, C.E., 2013. C<sub>3</sub> Poaceae and Restionaceae phytoliths as potential proxies for  
749 reconstructing winter rainfall in South Africa. *Quat. Int.* 287, 121-180.
- 750 Cordova, C., Avery, G., 2017. African savanna elephants and their vegetation associations in  
751 the Cape Region, South Africa: Opal phytoliths from dental calculus on prehistoric, historic  
752 and reserve elephants. *Quat. Int.* 443, 189-211.

- 753 Cordova, C.E., Kirsten, K.L., Scott, L., Meadows, M. and Lücke, A., 2019. Multi-proxy evidence  
754 of late-Holocene paleoenvironmental change at Princessvlei, South Africa: The effects of fire,  
755 herbivores, and humans. *Quaternary Science Reviews* 221, 105896.
- 756 Cordova, C.E., Scott, L., 2010. The potential of Poaceae, Cyperaceae, and Restionaceae  
757 phytoliths to reflect past environmental conditions in South Africa. *Palaecol. Afr.*, 107-133.
- 758 Diefendorf, A.F., Mueller, K.E., Wing, S.L., Koch, P.L., & Freeman, K.H. 2010. Global patterns  
759 in leaf <sup>13</sup>C discrimination and implications for studies of past and future climate. *Proceedings*  
760 *of the National Academy of Sciences*, 107, 5738-5743.
- 761 Faegri, K., Iversen, J., 1989. *Textbook of Pollen Analysis*, 4th edition. JohnWiley and Sons,  
762 New York.
- 763 Faith, J.T., Chase, B.M., Avery, D.M., 2018. Late Quaternary micromammals and the  
764 precipitation history of the southern Cape, South Africa. *Quat. Res.* 1–13.  
765 doi:10.1017/qua.2018.105.
- 766 Fischer, H., Fundel, F., Ruth, U., Twarloh, B., Wegner, A., Udisti, R., Becagli, S., Castellano, E.,  
767 Morganti, A., Severi, M., Wolff, E., Littot, G., Röthlisberger, R., Mulvaney, R., Hutterli, M.A.,  
768 Kaufmann, P., Federer, U., Lambert, F., Bigler, M., Hansson, M., Jonsell, U., de Angelis, M.,  
769 Boutron, C., Siggaard-Andersen, M.-L., Steffensen, J.P., Barbante, C., Gaspari, V., Gabrielli, P.,  
770 Wagenbach, D., 2007. Reconstruction of millennial changes in dust emission, transport and  
771 regional sea ice coverage using the deep EPICA ice cores from the Atlantic and Indian Ocean  
772 sector of Antarctica. *Earth Planet. Sci. Lett.* 260, 340-354.
- 773 Grimm, E. 2011. *TILIA Software, version 1.7.* 16. Springfield, IL: Illinois State Museum,  
774 Research and Collection Center.
- 775 Hogg, A.G., Hua, Q., Blackwell, P.G., Buck, C.E., Guilderson, T.P., Heaton, T.J., Niu, M., Palmer,  
776 J., Reimer, P.J., Reimer, R., Turney, C.S.M., Zimmerman, S.R.H., 2013. *ShCal13 Southern*

- 777 Hemisphere calibration, 0-50,000 cal yr BP. Radiocarbon 55(4),  
778 doi:10.2458/azu\_js\_rc.55.16783.
- 779 Lim, S., Chase, B.M., Chevalier, M., Reimer, P.J., 2016. 50,000 years of vegetation and climate  
780 change in the southern Namib Desert, Pella, South Africa. Palaeogeography,  
781 Palaeoclimatology. Palaeoecology 451, 197-209.
- 782 Martin, A.R.H. 1968. Pollen analysis of Groenvlei lake sediments, Knysna (South Africa).  
783 Review of Palaeobotany and Palynology 7, 107–144.
- 784 Mucina, L., Rutherford, M.C. 2006. The Vegetation of South Africa, Lesotho, and Swaziland,  
785 Strelitzia 19. South African National Biodiversity Institute, Pretoria.
- 786 Munsterman, M., Kerstholt, S. 1996. Sodium polytungstate, a new non-toxic alternative to  
787 bromoform in heavy liquid separation. Review of Palaeobotany and Palynology 91, 417-422.
- 788 Nielsen, S.H.H., Koç, N., Crosta, X. 2004. Holocene climate in the Atlantic sector of the  
789 Southern Ocean: controlled by insolation or oceanic circulation? Geology 32, 317–320.
- 790 O'Leary, M. H. 1988. Carbon isotopes in photosynthesis. Bioscience 38, 328-336.
- 791 Street-Perrott F. A. and Perrott, R. A. 1993. Holocene Vegetation, Lake Levels, and Climate of  
792 Africa. In: H. E. Wright, J. E. Kutzbach, T. Webb, W. F., Ruddiman, F. A. Street-Perrott, P. J.  
793 Bartlein. Global Climates since the Last Glacial Maximum. Chapter 13 pp. 318-356.
- 794 Stockmarr, J. 1971. Tablets with spores used in absolute pollen analysis. Pollen et Spores XIII,  
795 615-621.
- 796 Quick, L.J., Chase, B.M., Meadows, M.E., Scott, L., Reimer, P.J., 2011. A 19.5 kyr vegetation  
797 history from the central Cederberg Mountains, South Africa: Palynological evidence from rock  
798 hyrax middens. Palaeogeogr. Palaeoclimatol. Palaeoecol. 309, 253-270.
- 799 Quick, L.J., Carr, A.S., Meadows, M.E., Boom, A., Bateman, M.D., Roberts, D.L., Reimer, P.J.,  
800 Chase, B.M. 2015. A late Pleistocene-Holocene multi-proxy record of palaeoenvironmental

- 801 change from Still Bay, southern Cape coast, South Africa. *Journal of Quaternary Science*, 30  
802 (8), 870-885.
- 803 Quick, L., Carr, A.S., Meadows, M.E., Boom, A., Bateman, M.D., Roberts, D.L., Reimers, P.J.,  
804 Chase, B.M., 2016. A late Pleistocene-Holocene multi-proxy record of palaeoenvironmental  
805 change from Still Bay, southern Cape Coast, South Africa. *J. Quat. Sci.* 30, 870-885.
- 806 Quick, L.J., Chase, B.M., Wündsche, M., Kirsten, K.L., Chevalier, M., Mäusbacher, R., Meadows,  
807 M.E., Haberzettl, T., 2018. A high-resolution record of Holocene climate and vegetation  
808 dynamics from the southern Cape coast of South Africa: pollen and microcharcoal evidence  
809 from Eilandvlei. *J. Quat. Sci.* 33, 487-500.
- 810 Rebelo, A.G., Boucher, C., Helme, N., Mucina, L., Rutherford, M.C., 2006. Fynbos Biome. In:  
811 Mucina, L., Rutherford, M.C. (Eds.). *The Vegetation of South Africa, Lesotho, and Swaziland*,  
812 *Strelitzia* 19. South African National Biodiversity Institute, Pretoria, pp. 53-219.
- 813 Rundel, P. W., Esler, K. J., & Cowling, R. M. 1999. Ecological and phylogenetic patterns of  
814 carbon isotope discrimination in the winter-rainfall flora of the Richtersveld, South Africa.  
815 *Plant Ecology*, 142, 133-148.
- 816 Scholtz, A. 1986. *Palynological and Palaeobotanical Studies in the Southern Cape*.  
817 Stellenbosch, University of Stellenbosch.
- 818 Scott, L. 1996. Palynology of hyrax middens: 2000 years of palaeo-environmental history in  
819 Namibia. *Quaternary International* 33, 73-79.
- 820 Scott, L., Bousman, C.B., Nyakale, M. 2005. Holocene pollen from swamp, cave and hyrax dung  
821 deposits at Blydefontein (Kikvorsberge), Karoo, South Africa. *Quaternary International* 129:  
822 49-59.

- 823 Scott, L., Neumann, F.H., Brook, G.A., Bousman, C.B., E. Norström, E., Metwally, A.A. 2012.  
824 Terrestrial fossil Pollen Evidence of Climate Change during the last 26 Thousand Years in  
825 Southern Africa. *Quaternary Science Reviews* 32, 100- 118.
- 826 Scott, L., Sobol, M., Neumann, F.H., Gil Romera, G., Fernández-Jalvo, J., Bousman, C.B.,  
827 Horwitz, L.K., van Aardt, A.C. 2020. Late Quaternary palaeoenvironments in the central semi-  
828 arid region of South Africa from pollen in cave, pan, spring, stream and dung deposits.  
829 *Quaternary International* (submitted).
- 830 Scott, L. and Vogel, J.C. 2000. Evidence for environmental conditions during the last 20,000  
831 years in Southern Africa from <sup>13</sup>C in fossil hyrax dung. *Global and Planetary Change* 26(1-3),  
832 207-215.
- 833 Scott, L., Woodborne, S., 2007a. Pollen analysis and dating of late quaternary faecal deposits  
834 (hyraceum) in the Cederberg, Western Cape, South Africa. *Rev. Palaeobot. Palynol.* 144, 123-  
835 134.
- 836 Scott, L., Woodborne, S., 2007b. Vegetation history inferred from pollen in Late Quaternary  
837 faecal deposits (hyraceum) in the Cape winter-rain region and its bearing on past climates in  
838 South Africa. *Quat. Sci. Rev.* 26, 941-953.
- 839 Scott, L., Sobol, M., Neumann, F. H., Gil Romera, G., Fernández-Jalvo, Y, Bousman, C. B.,  
840 Horwitz, L. K., van Aardt, A. C. 2020. Late Quaternary palaeoenvironments in the central semi-  
841 arid region of South Africa from pollen in cave, pan, spring, stream and dung deposits,  
842 *Quaternary International* (<https://doi.org/10.1016/j.quaint.2020.10.065>).
- 843 Taljaard, J.J., 1966. *Atmospheric Circulation Systems, Synoptic Climatology and Weather*  
844 *Phenomena of South Africa. Part 6: Rainfall in South Africa.* South African Weather Bureau.  
845 Technical paper 32. 100 pp.

- 846 Talma, A.S., Vogel, J.C., 1992. Late quaternary paleotemperatures derived from aspeleothem  
847 from Cango caves, Cape Province, South Africa. *Quat. Res.* 37 (2), 203-213.
- 848 Thackeray, J.F., 1987. Late Quaternary environmental changes inferred from small  
849 mammalian fauna, southern Africa. *Climatic Change* 10, 285-305.
- 850 Tyson, P.D., Preston-Whyte, R.A., 2000. *The Weather and Climate of Southern Africa*. Oxford  
851 University Press, Cape Town, 396pp.
- 852 Valsecchi, V., Chase, B.M., Slingsby, J.A., Carr, A.S., Quick, L.J., Meadows, M.E., Cheddadi, R.,  
853 Reimer, P.J., 2013. A high resolution 15,600-year pollen and microcharcoal record from the  
854 Cederberg Mountains, South Africa. *Palaeogeogr. Palaeoclimatol. Palaeoecol.* 387, 6-16.
- 855 van Zinderen Bakker, E.M., 1976. The evolution of late Quaternary paleoclimates of Southern  
856 Africa. *Palaeoecology of Africa* 9, 160-202.
- 857 Vogel, J.C., Fuls, A., Ellis, R.P., 1978. The geographical distribution of Kranz grasses in South  
858 Africa. *S. Afr. J. Sci.* 74, 209-215.